

DISK EVOLUTION IN THE THREE NEARBY STAR-FORMING REGIONS OF TAURUS, CHAMAELEON, AND OPHIUCHUS

E. Furlan^{1,2}, Dan M. Watson³, M. K. McClure^{3,4}, P. Manoj³, C. Espaillat⁴, P. D'Alessio⁵, N. Calvet⁴, K. H. Kim³, B. A. Sargent³, W. J. Forrest³, L. Hartmann⁴

To appear in ApJ

ABSTRACT

We analyze samples of Spitzer Infrared Spectrograph (IRS) spectra of T Tauri stars in the Ophiuchus, Taurus, and Chamaeleon I star-forming regions, whose median ages lie in the < 1 to 2 Myr range. The median mid-infrared spectra of objects in these three regions are similar in shape, suggesting, on average, similar disk structures. When normalized to the same stellar luminosity, the medians follow each other closely, implying comparable mid-infrared excess emission from the circumstellar disks. We use the spectral index between 13 and 31 μm and the equivalent width of the 10 μm silicate emission feature to identify objects whose disk composition departs from that of a continuous, optically thick accretion disk. Transitional disks, whose steep 13 – 31 μm spectral slope and near-IR excess deficit reveal inner disk clearing, occur with about the same frequency of a few percent in all three regions. Objects with unusually large 10 μm equivalent widths are more common (20–30%); they could reveal the presence of disk gaps filled with optically thin dust. Based on their medians and fraction of evolved disks, T Tauri stars in Taurus and Chamaeleon I are very alike. Disk evolution sets in early, since already the youngest region, the Ophiuchus core (L1688), has more settled disks with larger grains. Our results indicate that protoplanetary disks show clear signs of dust evolution at an age of a few Myr, even as early as ~ 1 Myr, but age is not the only factor determining the degree of evolution during the first few million years of a disk's lifetime.

Subject headings: circumstellar matter | stars: formation | stars: pre-main sequence | infrared: stars

1. INTRODUCTION

Protoplanetary disks around pre-main-sequence stars are known to dissipate over the course of a few million years; at an age of ~ 10 Myr, very few objects are still surrounded by primordial disks (Jayawardhana et al. 1999; Haisch et al. 2001; Sicilia-Aguilar et al. 2006; Jayawardhana et al. 2006; Hernandez et al. 2006). During the first 1–2 Myr, disks already experience significant evolution: dust grains have been shown to grow and settle towards the disk mid-plane (e.g., Miyake & Nakagawa 1995; Apai et al. 2005; D'Alessio et al. 2006; Furlan et al. 2005, 2006), to be partly processed into crystalline form (e.g., Meus et al. 2003; Kessler-Silacci et al. 2006; Sargent et al. 2006, 2009), and to be removed from certain radial regions in a disk, likely due to the gravitational interactions with a companion that formed in the disk, such as a newly formed planet (e.g., Skrutskie et al. 1990; Calvet et al. 2005; Espaillat et al. 2008). By understanding the pro-

cesses occurring in a protoplanetary disk, we gain insights into disk clearing and planet formation mechanisms; observing such disks at the onset of these processes allows us to discriminate better the degree to which each process contributes to disk evolution.

Close to the Sun, at a distance of about 150 pc (Bertout et al. 1999), lie three star-forming regions whose ages are thought to fall into the 1–2 Myr range: Taurus-Auriga, Ophiuchus, and Chamaeleon I. Ophiuchus is the youngest (< 1 Myr; Luhman & Rieke 1999) and most embedded of the three; its core region (L1688; $\sim 30^\circ$) has a very high stellar concentration (e.g., Greene & Young 1992; Bontemps et al. 2001). Both Chamaeleon I and Taurus are less extinguished and crowded than Ophiuchus. Chamaeleon I has a median age of 2 Myr (Luhman 2004a), but a large age spread ranging from ~ 1 Myr up to 6 Myr (Luhman 2007), and it is somewhat older than Taurus, whose age is about 1 Myr, with a distribution of ages between 1 and several Myr (Kenyon & Hartmann 1995; Hartmann 2001; Luhman et al. 2003). The region surrounding the compact Ophiuchus core contains several young stellar objects (YSOs) that are less obscured and older than the Ophiuchus core region (Ichikawa & Nishida 1989; Chen et al. 1995; Wilking et al. 2005). Since the location in the H-R diagram of objects from this off-core region (see Wilking et al. 2005) is similar to that of members of Chamaeleon I (see Luhman 2007), these two regions have comparable ages (~ 2 Myr), independent of evolutionary models.

The majority of objects in the Ophiuchus, Taurus, and Chamaeleon I star-forming regions are T Tauri stars, which are initially surrounded by optically thick circum-

¹ NASA Astrobiology Institute, and Department of Physics and Astronomy, UCLA, 430 Portola Plaza, Los Angeles, CA 90095

² current address: JPL, Caltech, Mail Stop 264-767, 4800 Oak Grove Drive, Pasadena, CA 91109; E: lise.furlan@jpl.nasa.gov

³ Department of Physics and Astronomy, University of Rochester, Rochester, NY 14627; dmw@pas.rochester.edu, manoj@pas.rochester.edu, khkim@pas.rochester.edu, bsargent@pas.rochester.edu, forrest@pas.rochester.edu

⁴ Department of Astronomy, The University of Michigan, 500 Church St., 830 Dennison Bldg., Ann Arbor, MI 48109; melisma@umich.edu, coespa@umich.edu, ncalvet@umich.edu, hartm@umich.edu

⁵ Centro de Radioastronomía y Astrofísica, Universidad Nacional Autónoma de México, Apartado Postal 3-72 (Xangari), 58089 Morelia, Michoacán, México; p.dallessio@astroson.unam.mx

stellar disks that are accreting onto the star; during this stage, they are referred to as classical T Tauri stars. The dust in the disk causes an excess at infrared wavelengths, which decreases over time as the disk material is dissipated. The slope n of the spectral energy distribution (SED), F_{ν} / ν^n , measured between 2 and 25 μm , is used to classify systems at different evolutionary stages: Class II objects have $-2 < n < 0$ and are surrounded by protoplanetary disks, while Class III objects have $-3 < n < -2$ and thus have little or no circumstellar material left (Lada 1987; Adams et al. 1987; Andre & Montmerle 1994). Pre-main-sequence stars that do not display any accretion signatures are also known as weak-lined T Tauri stars.

The infrared excess from protoplanetary disks is emitted as optically thick, continuum emission from the dusty disk interior, and optically thin emission from dust in the disk surface layer, whose prominent signatures are silicate emission features at 10 and 18 μm . Thus, mid-infrared spectra are ideally suited to study these YSOs; they allow us to assess the degree of dust crystallization, grain growth and settling, and disk clearing, processes which, at an age of 1–2 Myr, are likely in their initial stages. Studying protoplanetary disks in the four regions mentioned above will lead to a better understanding of how the circumstellar material evolves and eventually dissipates, possibly giving rise to planetary systems like our own.

As part of a large survey of star-forming regions within 500 pc, our team has obtained several hundred 5–36 μm spectra of YSOs in the Taurus, Cham aeleon I, Ophiuchus core, and Ophiuchus σ -core regions using the Infrared Spectrograph⁶ (IRS; Houck et al. 2004) on board the Spitzer Space Telescope (Werner et al. 2004). These spectra are classified and presented in Furlan et al. (2006) (Taurus), Manoj et al. (in preparation) (Cham aeleon I), and McClore et al. (in preparation) (Ophiuchus). Here we analyze some two hundred Class II objects identified in those papers. In §2 we introduce our sample, observations, and data reduction and processing, in §3 we compare the median IRS spectra of our objects in Taurus, Cham aeleon I, and the Ophiuchus core region, in §4 we analyze indicators of disk structure and infer the degree of disk evolution in all four regions; finally, we discuss our results in §5 and give our conclusions in §6.

2. OBSERVATIONS

2.1. Sample Selection and Data Reduction

Our Taurus, Cham aeleon I, and Ophiuchus targets were observed as part of an IRS guaranteed-time program during IRS campaigns 3, 4, 12, 19, 20, 21, 22, 23, 29, and 30, which were scheduled from February 2004 to April 2006. The objects⁷ were originally selected from infrared catalogs of YSOs in these regions that were compiled before the launch of the Spitzer Space Telescope in 2003 (mainly the IRAS Faint Source and

Point Source Catalogs; the DENIS Database, 2nd release; the 2MASS Catalog; Wilking et al. 1989; Greene et al. 1994; Kenyon & Hartmann 1995; Barsony et al. 1997; Cambresy et al. 1998; Persi et al. 2000). The targets in the Ophiuchus σ -core region were chosen from Ichikawa & Nishida (1989) and Chen et al. (1995); about half are located in or close to the L1689 cloud, one object (IRS 60) lies in L1709, and the remaining objects are spread over a wider area. With the availability of the IRS spectra, several targets that previously had an only tentative classification could be identified as Class II objects⁸ (see Furlan et al. (2006); McClore et al. (in preparation); Manoj et al. (in preparation)). In Cham aeleon I, we also included a few very low-mass stars and brown dwarfs (spectral type & M5) from Luhman (2004a) and Luhman (2007), which were observed in IRS campaigns 32, 33, 41, and 42. Our sample consists of 85 Class II objects in Taurus, 69 in Cham aeleon I, 63 in L1688, and 15 in the Ophiuchus σ -core regions.

All targets were observed with either the two low-resolution IRS modules (Short-Low [SL] and Long-Low [LL], 5.2{14 μm and 14{38 μm , respectively, / 90) or the SL module and the two high-resolution modules (Short-High [SH] and Long-High [LH], 10{19 μm and 19{37 μm , respectively, / 600). In this way we obtained the full mid-infrared spectrum from 5 to 40 μm for each target. While in Taurus most objects were observed in mapping mode with 2–3-step maps on the target, in Ophiuchus and Cham aeleon I most objects were observed in staring mode. The spectra were extracted from the Spitzer Science Center’s basic calibrated data (BCD) products, either pipeline versions S13.2 or S14.0 (S16.1 for the few objects observed in campaigns 41 and 42), and using the IDL-based SMART package (Higdon et al. 2004). More details on our observing modes, as well as a description of our data reduction steps, can be found in Furlan et al. (2006); notes on the reduction of individual objects are mentioned in McClore et al. (in preparation) for Ophiuchus and in Manoj et al. (in preparation) for Cham aeleon I.

2.2. Extinction Corrections

Basic target properties, such as spectral type, extinction, and multiplicity information, were taken mainly from the literature (Tables 1–4). In some cases, optical extinction A_V values were not available or resulted in dereddened optical photometry inconsistent with the expected photospheric emission. For objects with such unknown or uncertain extinction that are located in Taurus or Cham aeleon I, we computed the extinction from the observed V–I, I–J, or J–H colors by applying Mathis’s extinction curve (Mathis 1990) for an R_V value of 3.1. For the former two colors, we adopted intrinsic photospheric colors from Kenyon & Hartmann (1995), while for the latter one, we assumed an intrinsic J–H color typical for a classical T Tauri star from Meyer et al. (1997) (i.e., a typical J–H color defined by the CTTS locus). In a few cases we slightly adjusted the derived A_V values to

⁶ The IRS was a collaborative venture between Cornell University and Ball Aerospace Corporation funded by NASA through the Jet Propulsion Laboratory and the Ames Research Center.

⁷ A table, which lists object names and coordinates, is available in the electronic version of the journal; the first few lines of this table are shown in the Appendix.

⁸ Note that in Ophiuchus, where extinction is typically high, our Class II sample consists of systems that were identified based on the dominance of disk emission and not necessarily on their observed 2–25 μm spectral slope (see McClore et al. (in preparation) for details).

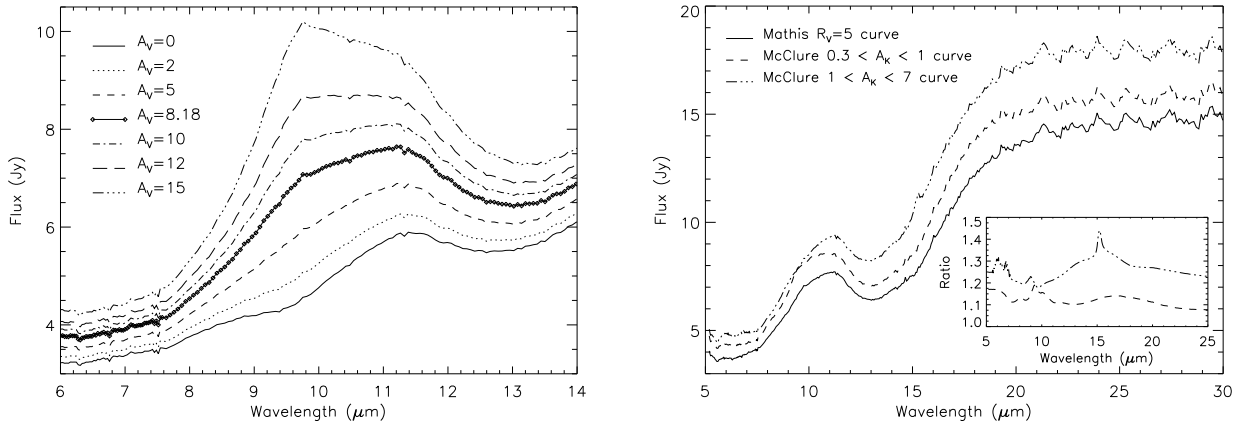


Fig. 1. Reddening correction for T 42, located in Cham aeleon I. Left: The spectrum for $A_V = 0$ is the original IRS spectrum, while the other spectra were dereddened using Mathis’s extinction curve and successively larger A_V values (from bottom to top); the actual extinction of T 42 is $A_V = 8.18$. Right: The IRS spectrum was dereddened assuming $A_V = 8.18$ and the three different extinction curves used in this paper; the spectrum in the middle is the one we adopted. The inset shows the ratio of the spectra dereddened with the McClure curves and the one obtained from dereddening with the Mathis’s curve.

obtain agreement between observed and expected photospheric colors. For objects located in the more deeply embedded Ophiuchus region, McClure et al. (in preparation) derived uniform extinctions and uncertainties for the entire sample from observed colors (I–J, J–H, or H–K) by applying Mathis’s curve for $R_V = 5.0$ (this larger R_V value is more appropriate for dense, molecular clouds; Mathis 1990). These authors also obtained near-infrared spectra of most of the on-core targets and of several of the more embedded core objects to determine spectral types, extinctions, and multiplicity.

In order to create a consistent data set, we decided to adopt the same dereddening prescription for all our targets, even though extinction curves likely vary among star-forming regions. For small A_V values, extinction curves for molecular clouds are similar to those for the diffuse interstellar medium (ISM), but for $A_V \geq 12$ there are clear deviations (Whittet et al. 1988; Chiar et al. 2007). Applying an ISM extinction curve like the Mathis curve to objects suffering from larger extinctions causes an overcorrection of the silicate emission feature at $9.8 \mu\text{m}$, resulting in a feature that is sharply peaked at that wavelength, and a $20/10 \mu\text{m}$ band ratio that is smaller than typical values for amorphous silicates (≈ 0.4 ; Dorschner et al. 1995). For example, Figure 1 (left panel) shows the silicate feature of T 42, a Class II object in Cham aeleon I. The original IRS spectrum displays a depression between 9 and $10 \mu\text{m}$ caused by extinction along the line of sight; when correcting the spectrum for reddening using Mathis’s curve, the absorption disappears. Using the extinction value determined for T 42, $A_V = 8.2$, and dereddening the spectrum, the silicate emission feature appears more square; applying an even larger reddening correction will cause a larger increase around $9.7 \mu\text{m}$ (where the correction applied by the Mathis curve is largest), resulting in a sharper silicate feature.

Studying background objects in molecular clouds, McClure (2009) found that already an A_V value of 3 resulted in a mid-infrared extinction curve that was different from the Mathis curve; at A_V values larger than about 9, the extinction curves converged. McClure (2009) derived two new extinction curves for the $A_V \leq 3$ regime, one for $3 < A_V < 9$ ($0.3 < A_K < 1$) and one for

$A_V \geq 9$ (the A_V values quoted here assume $R_V = 3.1$). The effect of applying different extinction curves to the IRS spectrum is shown in Figure 1 (right panel); the McClure curves cause a larger correction than Mathis’s law, with larger differences at wavelengths where ice absorptions play a role (see McClure (2009) for details).

We therefore adopted three different extinction curves to deredden our data, which were applied depending on the A_V value of our targets: we used a spline fit to the Mathis $R_V = 5.0$ curve for objects with $A_V < 3$, and the two McClure curves for objects with $A_V \geq 3$. Since the Mathis and McClure laws are given in $A = A_J$ and $A = A_K$, respectively, we converted the A_V values in Tables 1 to 4 to A_J and A_K by dividing by 3.55 and 9.0, respectively. These three curves were also used to deredden fluxes when constructing SEDs with ground-based optical photometry from the literature ($\times 4.2$). We note that for IRS spectra the correction for reddening using Mathis’s curve for $R_V = 3.1$ or 5.0 is the same, since the shape of this extinction curve does not vary with R_V for near- and mid-infrared wavelengths (Cardelli et al. 1989). Furthermore, most objects in Taurus and Cham aeleon I suffer from little extinction (the median A_V values for our samples are 1.5 and 2.7, respectively), so the details of the extinction curve have little impact on the resulting, dereddened spectra and SEDs. On the other hand, the median A_V value for the Ophiuchus core is 13.5, and thus uncertainties in the exact shape of the extinction curve make the dereddened Ophiuchus spectra somewhat more uncertain.

2.3. Sample Characteristics

Our Taurus and Cham aeleon I samples are representative for the Class II population of their respective star-forming regions. From a comparison with extensive membership lists (Kenyon & Hartmann 1995; Briceño et al. 2002; Luhmann 2004a), we conclude that, for spectral types earlier than M 0, our samples in these two regions are close to complete, while for later spectral types (up to M 6) we sample at least a few Class II objects in each spectral type bin.

Our sample in Ophiuchus is fairly representative, despite the high extinction in this region (which renders the determination of spectral types difficult); the posi-

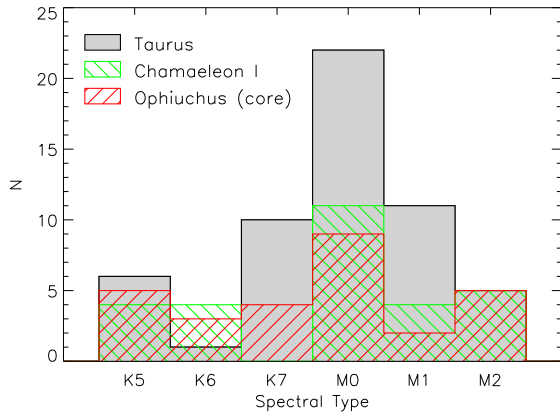


Fig. 2. Histogram for the distribution of spectral types among the objects entering the median in the Ophiuchus core, Taurus, and Chamaeleon I star-forming regions.

tion of our targets in L1688 is coincident with that of the CO gas that defines the L1688 cloud (Loren 1989). While we do not sample the most deeply embedded objects in the Ophiuchus core, the median A_V of 13.5 for our L1688 targets suggests that several, if not all, of them do belong to the young star-forming core. On the other hand, the targets in our Ophiuchus α -core sample (especially those not associated with any cloud) are likely members of a distinct, presumably older, population in this region, which has recently been surveyed with Spitzer (Padgett et al. 2008). Our very small sample in the α -core areas implies that our targets there are likely just the brightest members with an infrared excess.

3. COMPARISON OF MEDIAN IRS SPECTRA

In order to generally assess the state of evolution of circumstellar disks in our three star-forming regions, we computed the median IRS spectrum for the Class II objects in these regions. To avoid including objects with a large range in luminosities, we restricted the median to objects with spectral types from K5 to M2 (see D’Alessio et al. 1999). For Taurus, we used the spectra of 55 Class II objects, as in Furlan et al. (2006), while for Chamaeleon I and L1688, the spectra of 28 Class II objects in each region were included.

The distribution of spectral types of our median samples is shown in Figure 2. Despite a median spectral type of M0 for all three regions, in L1688 43% of objects have spectral types earlier than M0, while the this fraction amounts to 31% and 29% in Taurus and Chamaeleon I, respectively. Thus, the median of our Ophiuchus core targets is more representative for disks around slightly more massive stars than in Taurus and Chamaeleon I.

Before calculating the median for each region, we multiplied the dereddened IRS spectrum of each object by a scale factor to match the object’s dereddened H-band flux to the median H-band flux value of the region (near-IR magnitudes were taken from 2MASS [Skrutskie et al. (2006)]). The median IRS spectrum was then computed at each wavelength by using the scaled IRS spectra. The normalization at H results in an approximate normalization to the stellar luminosities, at the same

⁹ Note that the uncertainties in the number fractions quoted here and in the following sections are based on Poisson statistics and thus represent the standard margin of error.

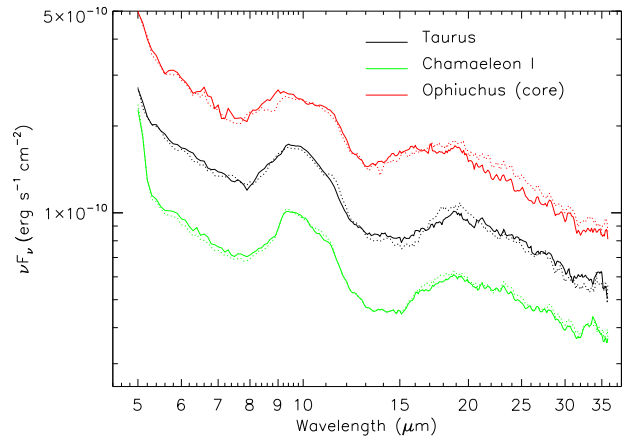


Fig. 3. The median IRS spectra for Taurus, Chamaeleon I and the Ophiuchus core; each median spectrum was normalized at a certain, dereddened median flux of the respective region: median H-band flux (solid lines) and median J-band flux (dotted lines).

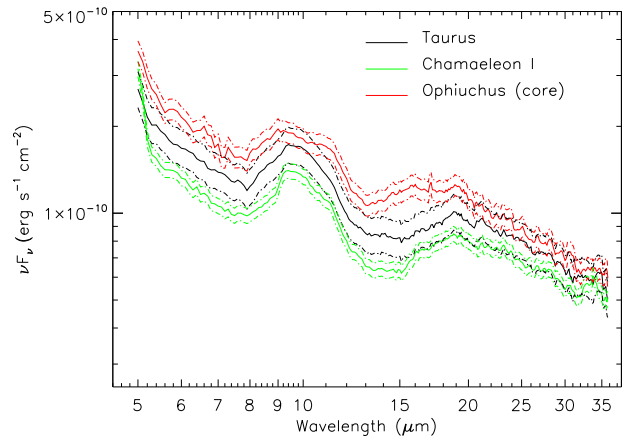


Fig. 4. The median IRS spectra for Taurus, the Ophiuchus core, and Chamaeleon I, normalized according to their mean relative distances (solid lines) and upper and lower distance limits (dash-dotted lines). See text for details.

time minimizing the effect of uncertain extinctions (see D’Alessio et al. 1999). The L1688 median carries a larger uncertainty due to the often uncertain spectral types and visual extinctions of the Ophiuchus sources.

In Figure 3 we show the median IRS spectra for the Class II objects in Taurus, Chamaeleon I, and the Ophiuchus core region. In order to check our results, we also computed the medians by normalizing at the dereddened J-band flux, which is more strongly affected by extinction corrections, but less by potential near-infrared excess from the circumstellar disks. The resulting medians are very similar to the ones normalized at H. For the remainder of this paper, when we refer to medians, we mean the medians that were internally normalized at H.

The fact that the Chamaeleon I and Ophiuchus medians are about 60% lower and higher, respectively, than the Taurus median can partly be attributed to differences in the distance to the various regions. Chamaeleon I is at 160–170 pc (Witt et al. 1997; Bertout et al. 1999), as opposed to 140 pc for Taurus (Bertout et al. 1999; Torres et al. 2007) and 120 pc for Ophiuchus (Loinard et al. 2008). Just due to this diversity, we would expect fluxes in Chamaeleon I to be a factor of 0.7 fainter and those in Ophiuchus to be a factor of 1.4

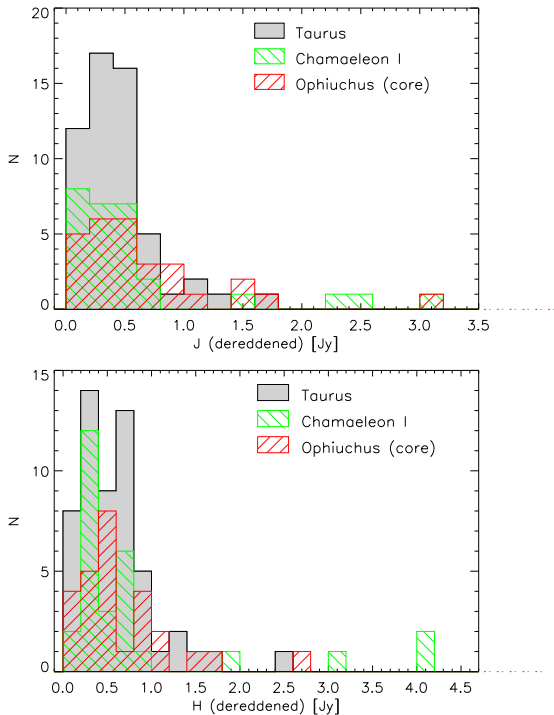


Fig. 5. | Histograms for the distribution of scaled, dereddened J- and H-band fluxes of the objects that entered the median calculation for the Taurus, Chamaeleon I, and the Ophiuchus core regions. The flux values were scaled according to the mean distance of the various regions with respect to Taurus.

brighter. This effect can be seen in Figure 4, where the median IRS spectra were multiplied by scale factors according to their relative distance to Taurus, first by using their mean distance (140 pc for Taurus, 120 pc for Ophiuchus, 165 pc for Chamaeleon I), then by considering the distance range typically quoted in the literature (130-150 pc for Taurus, 160-170 pc for Chamaeleon I; 115-125 pc for Ophiuchus; Bertout et al. 1999; Witt et al. 1997; Torres et al. 2007; Loinard et al. 2008).

After accounting for the larger distance, the Chamaeleon I median approaches the flux level of the Taurus median, but it is still somewhat lower (on average, at about 85% of the Taurus median if the mean distances are adopted). The distance-scaled median for the Ophiuchus core is still about 20% higher than the Taurus median. This could imply different intrinsic J- and H-band fluxes, with median near-IR fluxes highest in the Ophiuchus core, followed by Taurus and then Chamaeleon I.

Figure 5 shows the distribution of dereddened J- and H-band fluxes in the three regions, scaled according to their mean distance relative to Taurus to allow a direct comparison of the near-IR flux values. The median J- and H-band fluxes in Chamaeleon I are about a factor of 0.8 smaller than those in Taurus (the factor decreases to about 0.7-0.75 if the two outliers with the highest near-IR fluxes in Chamaeleon I are disregarded); therefore stars in Chamaeleon I are intrinsically fainter. On the other hand, the median J- and H-band fluxes of the Ophiuchus core region are higher than those of Taurus, by factors of 1.26 and 1.11, respectively (Figure 5). Thus, the intrinsic near-IR fluxes in L1688 are higher than in Taurus, and the higher flux level of the distance-scaled

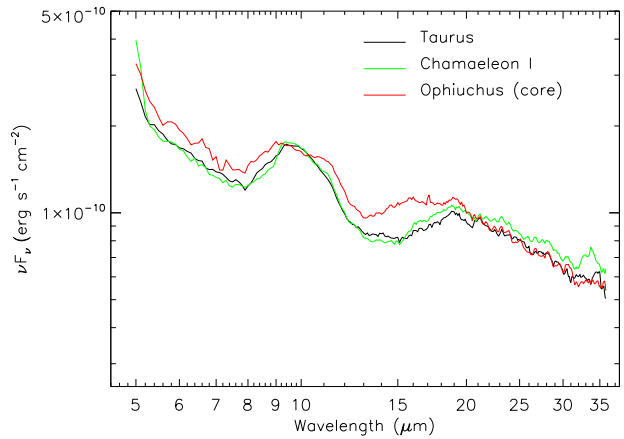


Fig. 6. | The median IRS spectra for Taurus, the Ophiuchus core, and Chamaeleon I, normalized at the dereddened H-band median flux of Taurus.

Ophiuchus median is likely caused by this difference in near-IR fluxes alone.

By normalizing the median IRS spectra of Taurus, the Ophiuchus core, and Chamaeleon I to a common H-band flux, which amounts to normalization to a common stellar luminosity, all three medians essentially overlap (Figure 6). Therefore, the mid-infrared excess emitted by circumstellar disks in these regions is similar and proportional to the stellar luminosity; this is expected in typical T Tauri disks, where irradiation by the central star dominates the disk heating (e.g., D'Alessio et al. 1999). The shapes of the medians are remarkably similar; on a relative scale, the median fluxes agree, on average, within a few %. However, in the 5-8 μ m range, the Ophiuchus median is about 15% higher than the Taurus median; this difference almost doubles in the 13-17 μ m region, with a maximum deviation of 35%. This is likely the result of applying the extinction curve for $A_V = 9$ from McClure (2009) to 3/4 of the targets that entered the Ophiuchus median; this extinction curve exhibits the largest deviation from the Mathis curve and causes a larger increase around 15 μ m (see the inset in the right panel of Figure 1). Despite some uncertainty in the applicable extinction curve for high-extinction regions such as the Ophiuchus core, the small differences we see among the medians of the three regions are likely real.

To compare the 10 μ m emission features, we first fit a continuum, defined as a 3rd, 4th, or 5th order polynomial, to the 5.6-7.9, 13.0-14.0, 14.5-15.5, 28.0-30.0 μ m wavelength regions of each spectrum with an associated spectral type of K5-M2. Then, this continuum fit was subtracted from the spectrum, and the result divided by the fit, which results in continuum-subtracted and -normalized 10 μ m emission features, i.e., we derived the emission of the optically thin dust alone. The median of these 10 μ m features for each region is shown in Figure 7. Also displayed in this figure is the average continuum-subtracted and -normalized silicate profile of LkCa 15 and GM Aur, two of the Taurus objects with the most pristine, or interstellar-like, silicate features (Sargent et al. 2009).

From Figure 7, it is clear that all three median 10 μ m features are wider than expected for small (sub- μ m) amorphous silicate grains, as are present in the interstellar medium, suggesting that grain growth occurred

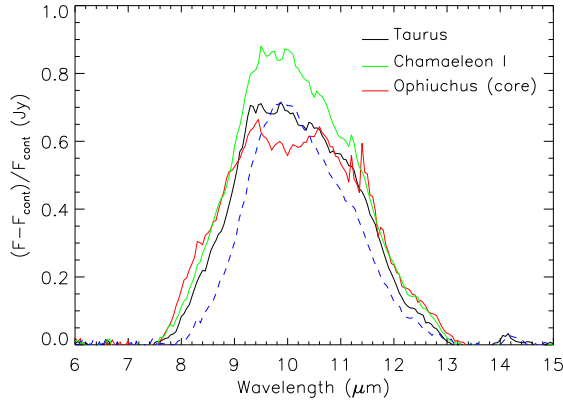


Fig. 7. The median IRS spectra for Taurus, Chamaeleon I and the Ophiuchus core around the 10 μm silicate emission feature, after subtraction and division by a continuum fit. The dashed blue line represents the emission feature of small (sub- μm) amorphous silicates; it is the average continuum-subtracted and -normalized profile of LkCa 15 and GM Aur, scaled to the mean 9.8 μm flux of the three medians.

in most disks of all three regions. The medians of both L1688 and Chamaeleon I display a 10 μm feature that is somewhat more structured than the Taurus median and also wider on the short-wavelength side. This could be an indication of crystalline silicates, which have narrower and more complex emission features than amorphous silicates (e.g., Fabian et al. 2001; Sargent et al. 2006); in particular, enstatite and silica have strong features around 9 μm (Jager et al. 1998; Wehrich & Christensen 1996). The fact that the long-wavelength wing of the 10 μm feature is not wider for L1688 and Chamaeleon I as compared to Taurus suggests that objects in these two regions do not have, on average, larger grains than their counterparts in Taurus. These results are just tentative, since only a model of the silicate profiles will reveal the fractions of large and of crystalline grains, but we believe that the differences we see in the silicate profiles are real, given that the extinction curves we applied to our spectra do not introduce artifacts at 10 μm .

Figure 8 shows the median spectra scaled to a common H-band flux (the median of Taurus), together with the quartiles, which delineate the range where 50% of spectra lie. For all three regions, the quartiles span a comparable range in flux values, and medians and lower quartiles follow each other closely over nearly all wavelengths. In the Ophiuchus core region, the lower quartile almost matches that of Taurus, while the upper quartile is generally a bit higher in flux and decreases more sharply beyond about 22 μm . For Chamaeleon I, both the lower and upper quartiles agree very well with the Taurus ones over the 9–22 μm wavelength region. Beyond 22 μm , the quartiles of the Ophiuchus core and Chamaeleon I define a somewhat smaller range in flux values around the median than the Taurus quartiles. In Taurus, the lower quartile decreases more steeply than the upper quartile beyond about 25 μm . Overall, the lower quartiles are closer to the medians than the upper quartiles, signifying that fainter disks span a smaller range in infrared excess than the brighter disks.

4. COMPARISON OF SPECTRAL INDICES AND SILICATE FEATURE STRENGTH

4.1. Definitions and Models

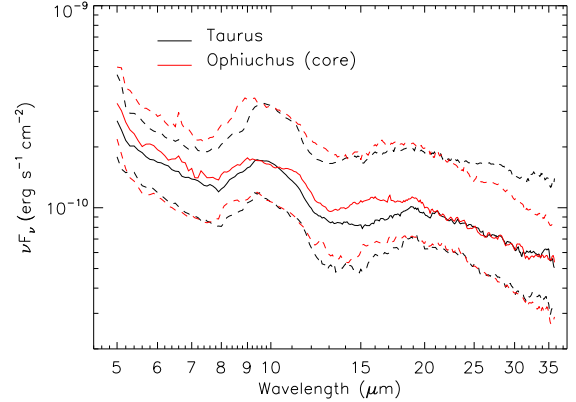
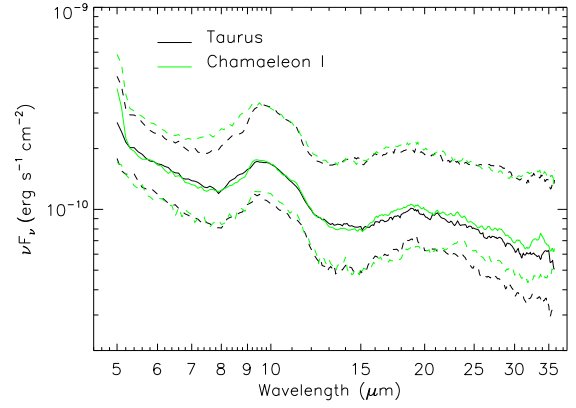


Fig. 8. The median IRS spectra (solid lines), normalized at the dereddened H-band median flux of Taurus, and their quartiles (dashed lines) for Taurus, Chamaeleon I and the Ophiuchus core.

Besides calculating the median mid-infrared spectra, which gauge the typical distribution of dust in circumstellar disks, we computed two quantities that probe dust evolution: the spectral index between 13 and 31 μm , $n_{13\ 31}$, and the equivalent width of the 10 μm silicate emission feature, $EW(10\ \mu\text{m})$ (see Watson et al. 2009).

The former quantity, formally expressed as

$$n_{13\ 31} = \frac{\log(F_{31}) - \log(F_{13})}{\log(\lambda_{31}) - \log(\lambda_{13})} \quad (1)$$

measures the slope of the spectral energy distribution (SED), i.e. F_ν / ν^n . We chose 13 and 31 μm as the endpoints for our slope determination, since these wavelengths are dominated by the longer-wavelength continuum emission from the optically thick disk. The fluxes at 13 and 31 μm were measured by averaging the flux in the 12.8–14.0 μm and 30.3–32.0 μm region, respectively; these bands exclude the broad silicate emission features at 10 and 20 μm generated in the optically thin disk atmosphere. As shown in D'Alessio et al. (2006) and Furlan et al. (2005, 2006), a steeper SED is indicative of increased dust settling, since a less flared disk intercepts less radiation from the central star, resulting in decreased heating and thus fainter continuum emission.

In order to measure the equivalent width of the 10 μm feature for each object, we first defined the continuum as a polynomial anchored in the 5.6–7.9, 13.0–14.0, 14.5–15.5, and 28.0–30.0 μm wavelength regions. Depending on the object, we adopted a third-, fourth-, or fifth-order polynomial to represent the continuum as a smooth curve extending from the wavelength region below 8 μm to

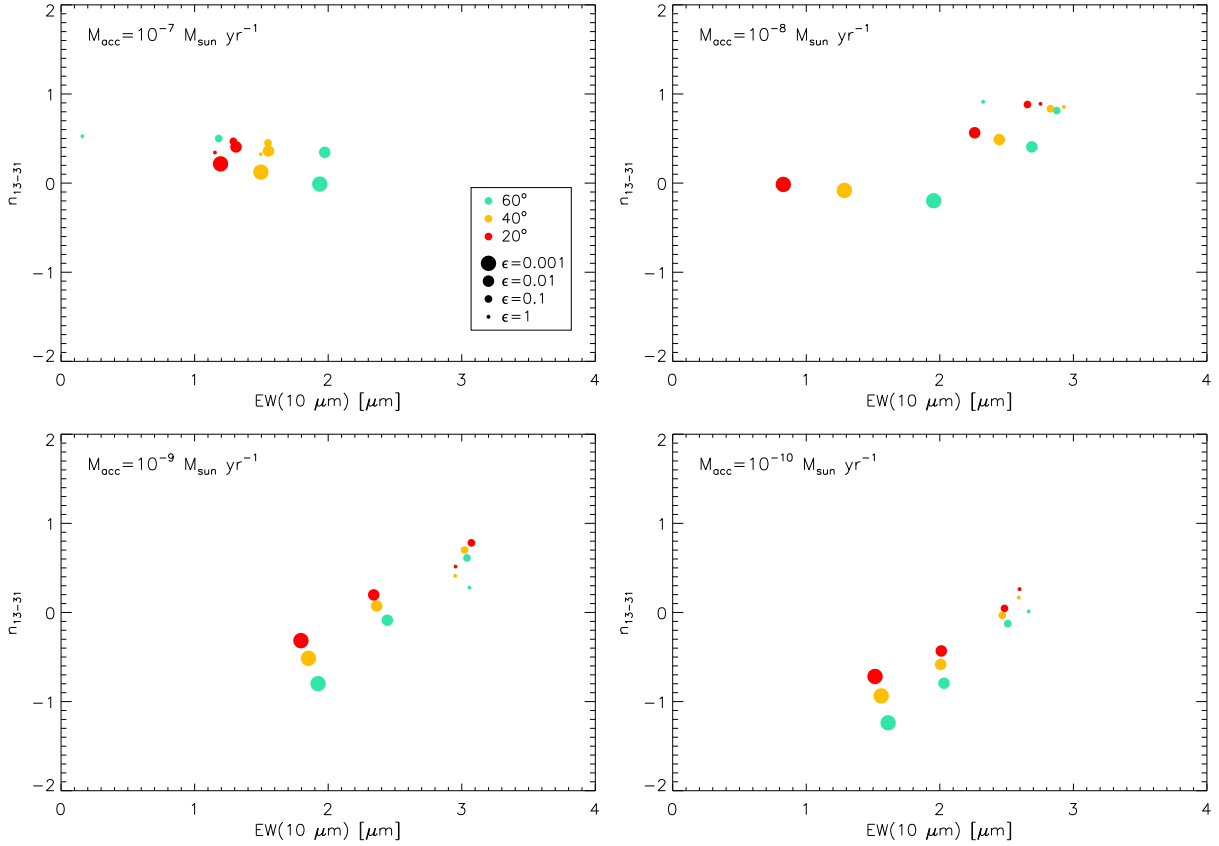


Fig. 9.— Spectral index between 13 and 31 μm versus the equivalent width of the 10 μm silicate emission feature for accretion disk models with mass accretion rates of 10^{-7} , 10^{-8} , 10^{-9} , and $10^{-10} M_{\odot} \text{yr}^{-1}$ (panels from top left to bottom right, respectively). The degree of dust settling increases according to symbol size. The colors code the inclination angle of the disk, as indicated in the label of the first panel.

that beyond 13 μm . Then we subtracted this continuum from the observed spectrum and divided the result by the continuum; this normalized, continuum-subtracted spectrum was finally integrated from 8 to 13 μm to yield the equivalent width of the 10 μm feature:

$$\text{EW}(10 \mu\text{m}) = \int_{8 \mu\text{m}}^{13 \mu\text{m}} \frac{F_{\lambda} - F_{\lambda, \text{cont}}}{F_{\lambda, \text{cont}}} d\lambda \quad (2)$$

This definition is actually the exact negative of the standard definition of equivalent width, which is positive for absorption lines and negative for emission lines. However, in order to facilitate representations of the equivalent width, we chose the above definition. The shape of the adopted continuum is often the main source of uncertainty of $\text{EW}(10 \mu\text{m})$; we took this into account when determining the overall uncertainty of our calculated $\text{EW}(10 \mu\text{m})$ values.

The $\text{EW}(10 \mu\text{m})$ is a measure for the amount of optically thin dust per area of optically thick disk. In a typical accretion disk, the optically thin emission is generated by small dust grains ($\sim 0.5 \mu\text{m}$) in the disk atmosphere (e.g., D’Alessio et al. 1999). It is the emission from these dust grains, and the energy released by accretion, that heats the lower disk layers; thus, the optically thin emission is tied to the optically thick continuum emission from the disk interior, and it will depend on the overall structure of the disk. As a disk evolves, dust grains are thought to grow and settle towards the disk midplane; the disk becomes less flared (smaller n_{13-31}),

and the strength of the silicate feature decreases (e.g., Dullemond & Dominik 2004, 2005; D’Alessio et al. 2006; Kessler-Silacci et al. 2006; Watson et al. 2009).

We determined typical ranges for n_{13-31} and $\text{EW}(10 \mu\text{m})$ by computing these quantities for a grid of accretion disk models around a $0.5 M_{\odot}$ star, following the same procedures as for the data. We only slightly modified the anchor regions for the continuum (7.0–7.9, 13.5–14.5, 28.0–30.0 μm) due to the different wavelength grid of the models. These models were calculated according to the methods of D’Alessio et al. (2006) (see also Espaillat (2009)); the vertical disk structure was derived self-consistently, resulting in a flared disk with a vertical inner rim at the dust sublimation radius (located where the dust reaches 1400 K). The dust in the disk was assumed to be composed of silicates and graphite (Draine & Lee 1984) and to scatter isotropically. The degree of dust settling was parameterized with ϵ , which is the ratio of the adopted dust-to-gas mass ratio in the upper disk layers relative to the standard dust-to-gas mass ratio of 1/100. A small value of ϵ implies depletion of small grains in the upper disk layers and an increase of larger grains close to the disk midplane.

The results of our n_{13-31} and $\text{EW}(10 \mu\text{m})$ calculations for the grid of accretion disk models are shown in Figure 9. For the models with a mass accretion rate of 10^{-7} to $10^{-8} M_{\odot} \text{yr}^{-1}$, the spread in n_{13-31} is mostly attributed to dust settling, with the more settled disks having a steeper SED slope. Dust settling also causes most of the spread in $\text{EW}(10 \mu\text{m})$ for the $10^{-8} M_{\odot} \text{yr}^{-1}$ models,

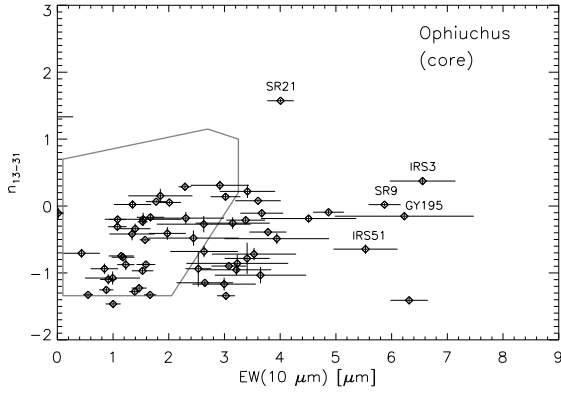


Fig. 10. | Spectral index between 13 and 31 μm versus the equivalent width of the 10 μm silicate emission feature for the Ophiuchus core region. The polygon specifies the region of typical accretion disks as derived from models. A few of the "outliers", which are discussed in the text, are labeled.

while for the higher mass accretion rate, this spread is mainly caused by different inclination angles. We note that at larger inclination angles ($\approx 75^\circ$; not shown), the silicate feature turns into absorption, especially for the more aged disks (i.e., $\tau > 1$), resulting in a small and eventually negative 10 μm equivalent width.

We obtain a somewhat smaller spread in $EW(10 \mu\text{m})$ for the models with a mass accretion rate of 10^9 to $10^{10} M_\odot \text{yr}^{-1}$ (Figure 9), but the range of n_{13-31} values is larger. The spread in spectral indices can be attributed to both dust settling and varying inclination angles. The more settled, highly inclined model disks approach the spectral index of $-4/3$, which is the value for an infinite, geometrically thin, optically thick disk.

The less settled model disks have the largest values for n_{13-31} and $EW(10 \mu\text{m})$ when their mass accretion rates amount to 10^8 to $10^9 M_\odot \text{yr}^{-1}$, which are representative figures for star-forming regions such as Taurus (Hartmann et al. 1998). In general, when dust grains grow and settle, the $EW(10 \mu\text{m})$ decreases; even though the presence of larger grains ($\approx 1\text{--}2 \mu\text{m}$) in the optically thin surface layer would increase the width of the silicate emission feature, its amplitude would be reduced such that the $EW(10 \mu\text{m})$ still decreases.

The range of disk models defines a region in the n_{13-31} versus $EW(10 \mu\text{m})$ plot which is occupied by typical accretion disks. This region extends from -1.33 to about 1.2 in n_{13-31} and from close to 0 to 2–3 (with higher values for more aged disks) in $EW(10 \mu\text{m})$; it is shown as the gray polygon in Figures 10 to 13. These latter figures show the spectral index from 13 to 31 μm and the equivalent width of the 10 μm feature calculated for the Class II objects in the Ophiuchus core region, Taurus, Chamaeleon I, and in the Ophiuchus off-core region, and are discussed below.

4.2. Class II Objects

As is apparent from Figures 10 to 12, most disks in L1688, Taurus, and Chamaeleon I have $n_{13-31} < 0$ (see also Fig. 14); the fraction is essentially the same in Taurus (80–10%) and L1688 (79–11%) and very similar in Chamaeleon I (71–10%). This indicates that the disk structures of typical objects in these three regions are, on average, comparable, as was gauged from their medians ($\times 3$), and that sedimentation starts early in the

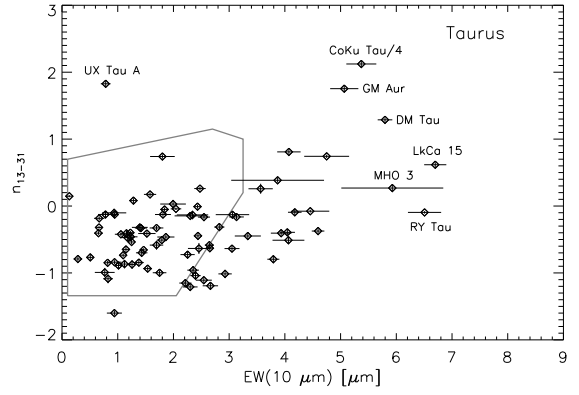


Fig. 11. | Same as Figure 10, but for the Taurus region.

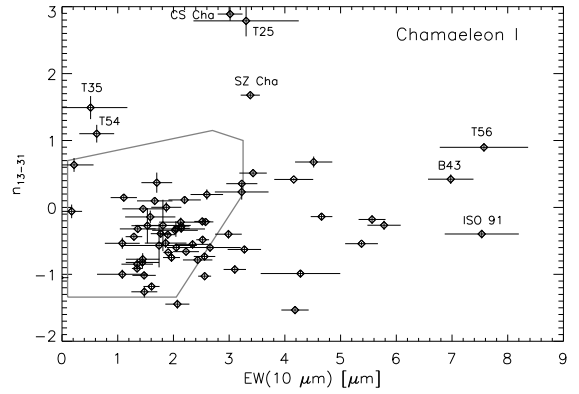


Fig. 12. | Same as Figure 10, but for the Chamaeleon I region.

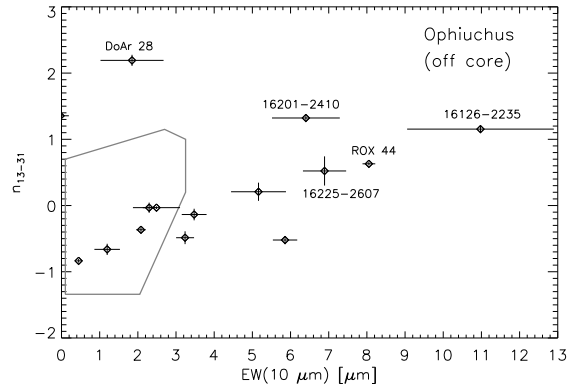


Fig. 13. | Same as Figure 10, but for the Ophiuchus off-core region.

lifetime of a protoplanetary disk, validating model predictions (Goldreich & Ward 1973; Chiang & Goldreich 1997; Dullemond & Dominik 2005). On the other hand, about half of our small sample of the Ophiuchus off-core region, which is similar in age to Chamaeleon I, has $n_{13-31} > 0$ (Fig. 13). Most of these objects typically have large 10 μm equivalent widths, too, suggesting an unusual disk structure.

In fact, each of these regions contains a substantial number of objects with $EW(10 \mu\text{m})$ values larger than expected from typical accretion disks (see Fig. 14 for the distribution of $EW(10 \mu\text{m})$ values). When counting the number of objects outside the region defined by the polygon in Figures 10 to 13 relative to the total num-

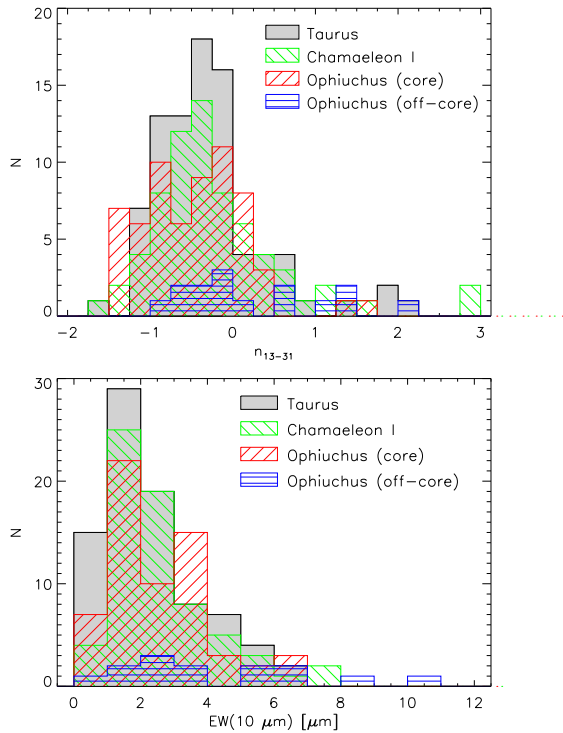


Fig. 14. Histograms for the distribution of n_{13-31} and $EW(10 \mu m)$ values for Taurus, Chamaeleon I, the Ophiuchus core and the Ophiuchus off-core regions.

ber of objects (not including objects whose $EW(10 \mu m)$ is negative due to poorly defined continua and silicate features), we derive that 35.7%, 27.6%, 29.6%, and 60.2% of Class II objects in the Ophiuchus core, Taurus, Chamaeleon I, and Ophiuchus off-core, respectively, have unexpectedly large silicate equivalent widths and/or larger n_{13-31} values. Considering the smaller sample size, the Ophiuchus off-core region has a marginally larger fraction of unusual objects than the other three regions. There is a lack of objects with very large n_{13-31} values in the Ophiuchus core region. We note that some of the uncertainties in $EW(10 \mu m)$ are relatively large; they are the result of ambiguity in the underlying continuum, which generally affects objects with strong $10 \mu m$ emission more, and of uncertain extinctions, but the latter to a minor extent and mostly for objects in L1688.

4.2.1. Outliers in n_{13-31}

We define the objects with steep spectral slopes from 13 to 31 μm ($n_{13-31} > 1$) as transitional disks. Despite being Class II objects, their SED rises sharply beyond about 10 μm , which is attributed to the presence of an inner disk wall bounding an inner disk hole whose deficit in small dust grains causes a decrease in near-infrared excess emission (Forrest et al. 2004; D'Alessio et al. 2005; Calvet et al. 2005; Espaillat et al. 2007a). A close, stellar companion could be responsible for the disk hole, and a luminous, embedded companion, whose SED peaks in the mid- to far-infrared, could create a transitional disk appearance (e.g., Duchêne et al. 2003). Therefore, interpretation of transitional disks in terms of disk evolution first requires identification of any close companions.

Ophiuchus core. Only one object associated with L1688 has an unusually large n_{13-31} value and reduced near-infrared excess emission: SR 21 (see Table 1 and Fig-

ure 15). Its IRS spectrum rises sharply beyond about 14 μm ; in addition, its silicate emission feature is superposed with PAH emission features, which are typical for disks around stars of earlier spectral type (e.g., Geers et al. 2006; SR 21 has a spectral type of F4), and therefore the $10 \mu m$ feature strength cannot be determined accurately. SR 21 is a 6.4^0 binary; the IRS spectrum contains the flux of both components, but the secondary is unlikely to contribute significantly at infrared wavelengths (Prato et al. 2003). The near-infrared excess seen in this object rules out a fully evacuated inner disk. Since H α measurements indicate that SR 21 is not accreting any more (Martín et al. 1998), the inner disk is likely dominated by dust, not gas. Models by Brown et al. (2007) require a gap between 0.45 and 18 AU to reproduce the observed SED of SR 21, with optically thick disk material remaining in the inner disk. Recent high-resolution, submillimeter images of this object reveal an inner cavity of ~ 37 AU in the dust continuum (Andrews et al. 2009), confirming the presence of the inner disk clearing.

Taurus. In Taurus, four objects have n_{13-31} values that are well above those found in typical accretion disks: CoKu Tau/4, UX Tau A, GM Aur, and DM Tau (Table 2 and Figure 15). All have been previously identified as transitional disks with different degrees of inner disk clearing, and they have been studied in detail by applying SED models (D'Alessio et al. 2005; Calvet et al. 2005; Espaillat et al. 2007b). The disks of CoKu Tau/4 and DM Tau are truncated at 10 and 3 AU, respectively, and the inner regions are depleted in dust (D'Alessio et al. 2005; Calvet et al. 2005). GM Aur and UX Tau A have inner disk holes at 24 and 56 AU, respectively, but optically thin dust within a few AU (GM Aur) or an optically thick ring of material at the dust sublimation radius (UX Tau A) (Calvet et al. 2005; Espaillat et al. 2007b). Recent submillimeter and millimeter interferometer maps of GM Aur confirm the inner disk hole of 20 AU (Hughes et al. 2009). Except for CoKu Tau/4, these objects are accreting and do not have close companions with mass ratios larger than 0.1 over a 20–160 m as separation range (Kenyon et al. 1998; White & Ghez 2001; Ireland & Kraus 2008). Recent work suggests that CoKu Tau/4 is a close binary (Ireland & Kraus 2008), and therefore its inner disk clearing is not caused by disk evolution. This leaves three "real" transitional disks in Taurus.

Chamaeleon I. In Chamaeleon I, there are five objects with a deficit of near-infrared excess emission and large n_{13-31} values: CS Cha, T 25, SZ Cha, T 35, and T 54 (Table 3 and Figure 15; see also Kim et al. 2009). CS Cha is a transitional disk similar to GM Aur, with some optically thin dust in the inner disk region (Espaillat et al. 2007a). Despite the recent discovery that it is a close binary system ($\sim 0.1^0$; Guenther et al. 2007), the fact that its inner hole is ~ 43 AU in size (Espaillat et al. 2007a) suggests that the binary might not be the only agent clearing out the inner disk of CS Cha. T 25 and T 54 somewhat resemble CS Cha; their emission is photospheric below about 10 μm and rises beyond 15 μm . T 25 is a single star and likely not accreting (Luhman 2004a; Lafrenière et al. 2008), implying that disk evolution might be responsible for the inner disk hole. T 54 is also not accreting (Feigelson & Kriss 1989); instead of

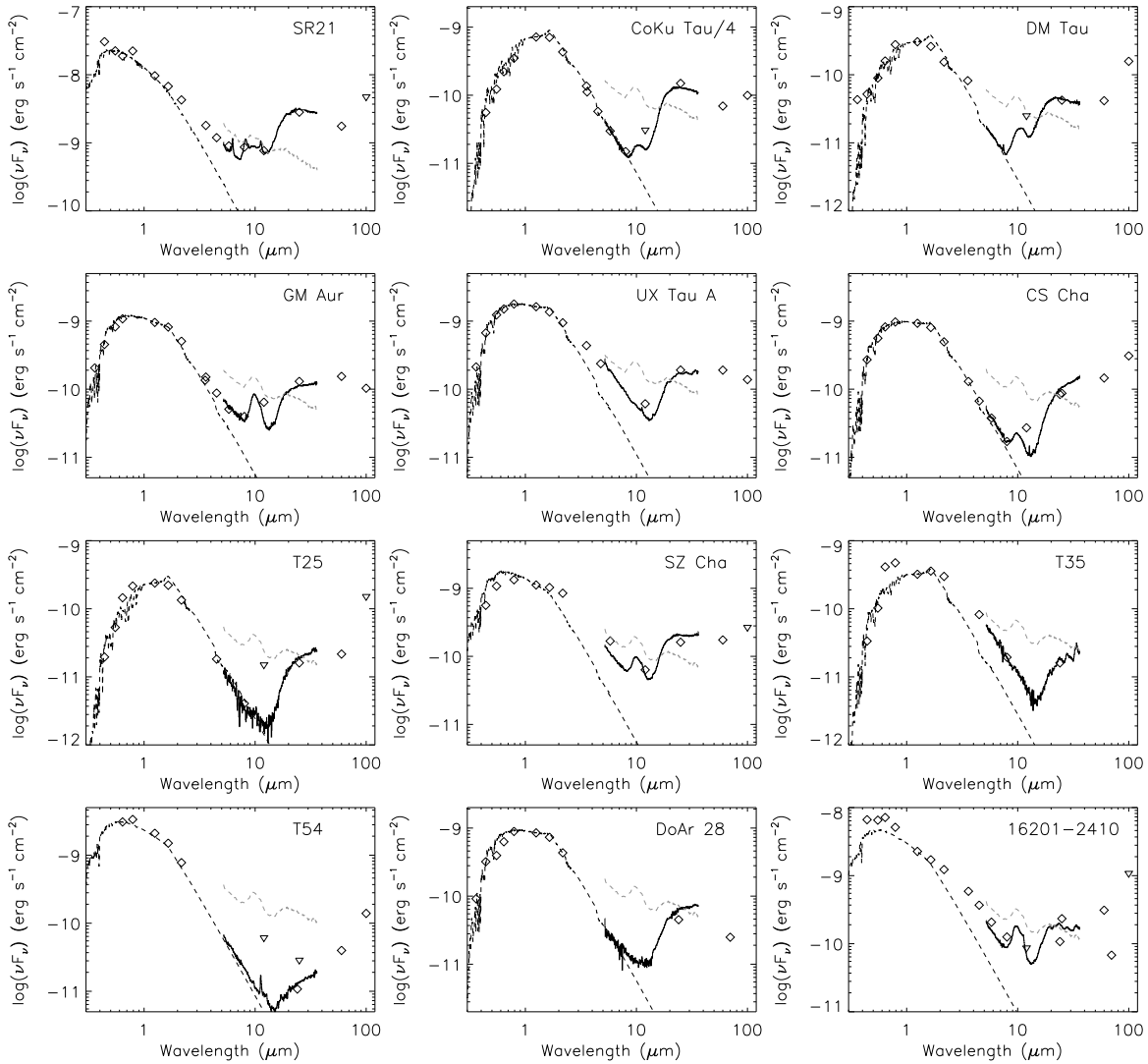


Fig. 15. | The dereddened SEDs of objects with unusually large n_{13-31} values (i.e., larger than expected from accretion disk models); the photospheres are represented by Kurucz model atmospheres with solar metallicity, $\log(g) = 3.5$, and different effective temperatures: $T_e = 6500$ K (SR21), $T_e = 3625$ K (CoKu Tau/4, T25), $T_e = 3750$ K (DM Tau), $T_e = 4750$ K (GM Aur), $T_e = 4375$ K (UX Tau A, DoAr 28), $T_e = 4250$ K (CS Cha), $T_e = 5250$ K (SZ Cha), $T_e = 3875$ K (T35), $T_e = 5500$ K (T54), and $T_e = 6000$ K (16201-2410). The photometry was adopted from the literature, and the data were dereddened as explained in the text. The dashed gray lines represent the medians of the Ophiuchus core (for SR21), of Taurus (for CoKu Tau/4, DM Tau, GM Aur, UX Tau A), and of Chamæleon I for the remaining objects, normalized at the H-band flux of each object. The Chamæleon I median was used also for the Ophiuchus α -core targets, since these two regions are of similar age.

silicate emission, it displays an 11–13 μ m PAH complex, and its spectral slope beyond 13 μ m is shallower than that of the other transitional disks. Since it has a companion at a separation of 0.27^{00} (Ghez et al. 1997), the inner disk is likely cleared by the binary. Both SZ Cha and T35 have some near-infrared excess emission and are also still accreting (Gauvin & Strom 1992; Luhman 2004a), suggesting the presence of optically thick material in the inner disk, as is the case for UX Tau A (Espaillat et al. 2007b). While T35 is probably a single star (Lafrenière et al. 2008), SZ Cha has two “companions”, one at 5.3^{00} and the other at 12.5^{00} (Ghez et al. 1997); however, these two objects are not confirmed members of Chamæleon I (Luhman 2007). Therefore, we recognize four transitional disks in Chamæleon I whose inner clearings are likely caused by disk evolution.

Ophiuchus α -core. Finally, we identify two objects in the Ophiuchus α -core region with a large 13–31 μ m spec-

tral index and low near-infrared excess emission: DoAr 28 and IRAS 16201-2410 (Table 4 and Figure 15). The former object lies 0.6° north of the L1688 cloud and is not associated with any of the filamentary clouds in Ophiuchus (e.g., Ratzka et al. 2005), while the latter one lies about 0.5° to the west of the main L1688 cloud. The SED of DoAr 28 is reminiscent of that of transitional disks with inner regions devoid of dust, like DM Tau or T25, but it might have a slight excess in the 5–8 μ m region. Since its H α emission indicates that it is still accreting (Cohen & Kuhi 1979), the inner disk, while depleted in dust, likely contains gas. It does not have a companion (the upper limit for the brightness ratio relative to the primary is 0.04 at 0.15^{00} ; Ratzka et al. 2005), and therefore its disk structure can probably be seen as an indication of disk evolution. The IRS spectrum of IRAS 16201-2410 shows a strong silicate emission feature in addition to the steep rise beyond about 14 μ m. Since, as

opposed to DOAr 28, it has some excess at near-infrared wavelengths, the inner disk is not fully cleared of dust. Recent near-infrared observations revealed that it has a companion at a projected separation of $2''$ (McClore et al., in preparation); since this companion seems to be very embedded, it could be responsible for a (small) fraction of the long-wavelength excess.

Three more objects have large n_{13-31} values, but display no silicate emission feature: IRS48 in L1688, CU Cha in Chamaeleon I, and IRAS 16156-2358 in the Ophiuchus σ -core (Figure 16). Their SEDs show numerous PAH features and a steep increase beyond about $15 \mu\text{m}$; while CU Cha and IRAS 16156-2358 have significant near-infrared excess, IRS48 displays no excess below $2 \mu\text{m}$. These objects are considered Herbig Ae/Be stars, given their early spectral type (A0 for IRS48, B9.5 for CU Cha, and F0 for IRAS 16156-2358).

Models of CU Cha showed that, while the near-infrared excess can be attributed to the puffed-up inner rim at the dust destruction radius, the rise in the SED in the 20–30 μm region is due to the aring disk that reemerges from the shadow behind the rim (Douchet et al. 2007). A similar disk structure could apply to IRAS 16156-2358; in addition, the steep rise of its SED beyond $15 \mu\text{m}$ could be partly due to a companion $4''$ to the south, which is fainter than the primary at $2.2 \mu\text{m}$ (M ASS, Skrutskie et al. 2006), but whose mid-infrared flux is not known. Therefore, despite the large n_{13-31} values, CU Cha and IRAS 16156-2358 likely do not belong to the transitional disk category.

On the other hand, the lack of near-IR excess emission and the presence of strong PAH features in IRS48 are consistent with observations of Geers et al. (2007), who resolved a gap with a radius of 30 AU in their $18.7 \mu\text{m}$ image of this object, but found that the PAH emission filled the gap region. Therefore, IRS48 seems to have a transitional disk structure, with a lack of small dust grains in the inner disk regions, but with some hot dust still present close to the star (Geers et al. 2007).

The frequency of disks in a transitional stage, based on n_{13-31} values, is comparable in all four regions and amounts to a few %. It is most uncertain in the Ophiuchus σ -core region with $13.3 \pm 9.4\%$, since the sample size is very small. The fraction of transitional disks in L1688 amounts to $3.2 \pm 2.2\%$; we note that L1688 lacks any disks with substantially cleared inner regions that would result in a severe deficit of infrared excess out to $8 \mu\text{m}$. The transitional disk fraction in Chamaeleon I ($5.8 \pm 2.9\%$) is similar to that in Taurus ($3.5 \pm 2.0\%$); the two star-forming environments are also alike.

When examining Figures 10 to 12 and Tables 1 to 3, a few Class II objects with particularly low n_{13-31} values are apparent: GY 292, SR 10, SR 20, and VSSG 5 in the Ophiuchus core, F04570+2520 in Taurus, and Hn 5 and T 51 in Chamaeleon I (see Figure 17 for their SEDs). The 13–31 μm spectral index of these objects is actually lower than the $\sim 4/3$ value expected for an in-nite, geometrically thin, optically thick disk (e.g., Adams et al. 1987). A possible cause for the steep SED slope is the outward truncation of the disk by the gravitational interaction of a close companion (Artymowicz & Lubow 1994; see also McClore et al. (2008) for a model of SR 20). GY 292, SR 10, F04570+2520, and Hn 5 do not have known companions (Ratzka et al. 2005; Furlan et al. 2006; Luhman

2004a), while SR 20 and VSSG 5 are sub-arcsecond binaries, with separations of $0.04''$ – $0.07''$ (Gez et al. 1995) and $0.15''$ (Ratzka et al. 2005), respectively, and T 51 is a $2''$ binary (Correia et al. 2006).

4.2.2. Outliers in EW ($10 \mu\text{m}$)

While the objects with steep SEDs between 13 and $31 \mu\text{m}$ have disks whose inner regions are depleted in small dust grains to different degrees, the objects with large $10 \mu\text{m}$ equivalent widths, but more typical n_{13-31} values, are more difficult to explain. The optically thin emission is enhanced above levels found for accretion disks in hydrostatic equilibrium. Therefore, the ratio of the projected area of the optically thin medium to that of the optically thick region must be larger than in a typical accretion disk. This can be achieved by either increasing the amount or emitting area of the optically thin dust, or by decreasing the continuum emission generated by the optically thick disk regions, but leaving the optically thin emission unchanged.

The most prominent outliers in terms of EW ($10 \mu\text{m}$) are found in Chamaeleon I and the Ophiuchus σ -core: T 56, ISO 91, and B 43 in the former, and IRAS 16126-2235, 16225-2607, and ROX 44 in the latter (see Figure 18). Of the three σ -core targets, only ROX 44 is associated with a cloud, L1689. Except for IRAS 16126-2235, which is a $1.9''$ binary (Jensen et al. 2004), these objects do not have known companions. Their SEDs display a deficit in near-infrared excess emission, a strong silicate emission feature at $10 \mu\text{m}$, and a rising SED beyond $15 \mu\text{m}$, somewhat reminiscent of transitional disks (Figure 20). In fact, their n_{13-31} values, while lower than those of transitional disks, lie in a range rarely occupied by typical accretion disks. The decreased levels of near-infrared excess emission indicate that their inner disks must be depleted in dust, and the rise in the SED at $15 \mu\text{m}$ might suggest the presence of some type of inner disk wall.

In the Ophiuchus core region, IRS 3, GY 195, SR 9, IRS 51, and GY 292 are notable outliers in EW ($10 \mu\text{m}$), while in Taurus LkCa 15, RY Tau, and MHO 3 share this characteristic (Figure 19). While GY 195, GY 292, SR 9, and LkCa 15 have decreased near-infrared excess emission, similar to the outliers in Chamaeleon I and the Ophiuchus σ -core, IRS 3, IRS 51, MHO 3, and RY Tau emit above median levels for their respective star-forming regions over the entire IRS wavelength range (Figure 20).

IRS 3 is a $0.66''$ binary with a flux ratio of 0.3 at $2.2 \mu\text{m}$ (Ratzka et al. 2005), but it is not known to what extent the secondary contributes to the infrared excess. SR 9 also has a companion at a separation of $0.64''$, but its flux ratio of 0.06 relative to the primary at $2.2 \mu\text{m}$ (Ratzka et al. 2005) renders it unlikely to significantly contribute at infrared wavelengths. IRS 51 is a binary, too, whose secondary at a distance of $1.65''$ is very faint (flux ratio of 0.04 at $2.2 \mu\text{m}$; Ratzka et al. 2005). Interestingly, GY 292 has both a large EW ($10 \mu\text{m}$) and a 13–31 μm spectral index somewhat below $-4/3$; therefore, its outer disk might be truncated, while its inner disk shares some of the properties of the other EW ($10 \mu\text{m}$) outliers.

RY Tau is the only object among the sample of EW ($10 \mu\text{m}$) outliers with an early spectral type (G1; see Table 2). It might have a very close companion, at a separation of at least 24 mas (Bertout et al. 1999). Based on a dip in its mid-infrared SED, Marsh & Mahoney (1992)

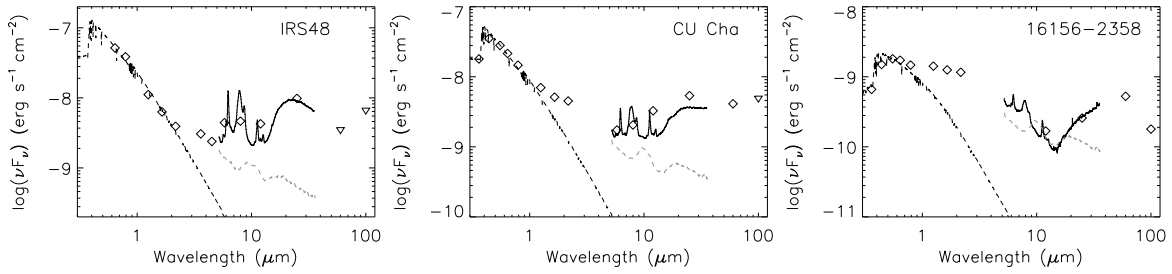


Fig. 16. | The dereddened SEDs of three Herbig Ae/Be stars with large n_{13-31} values; the photospheres are represented by Kurucz model atmospheres with solar metallicity, $\log(g)=3.5$, and different effective temperatures: $T_e = 9500$ K (IRS48), $T_e = 10000$ K (CU Cha), and $T_e = 7250$ K (16156-2358). The photometry for IRS48 was taken from various published catalogs (USNO, 2MASS, 2dFAS, IRAS), that for CU Cha was adopted from Hillenbrand et al. (1992), and for 16156-2358 from Vieira et al. (2003); the data were dereddened as explained in the text. The dashed gray lines represent the median of Ophiuchus (for IRS48) and of Chamaleon I (for the other two objects), normalized at the H-band flux of each object.

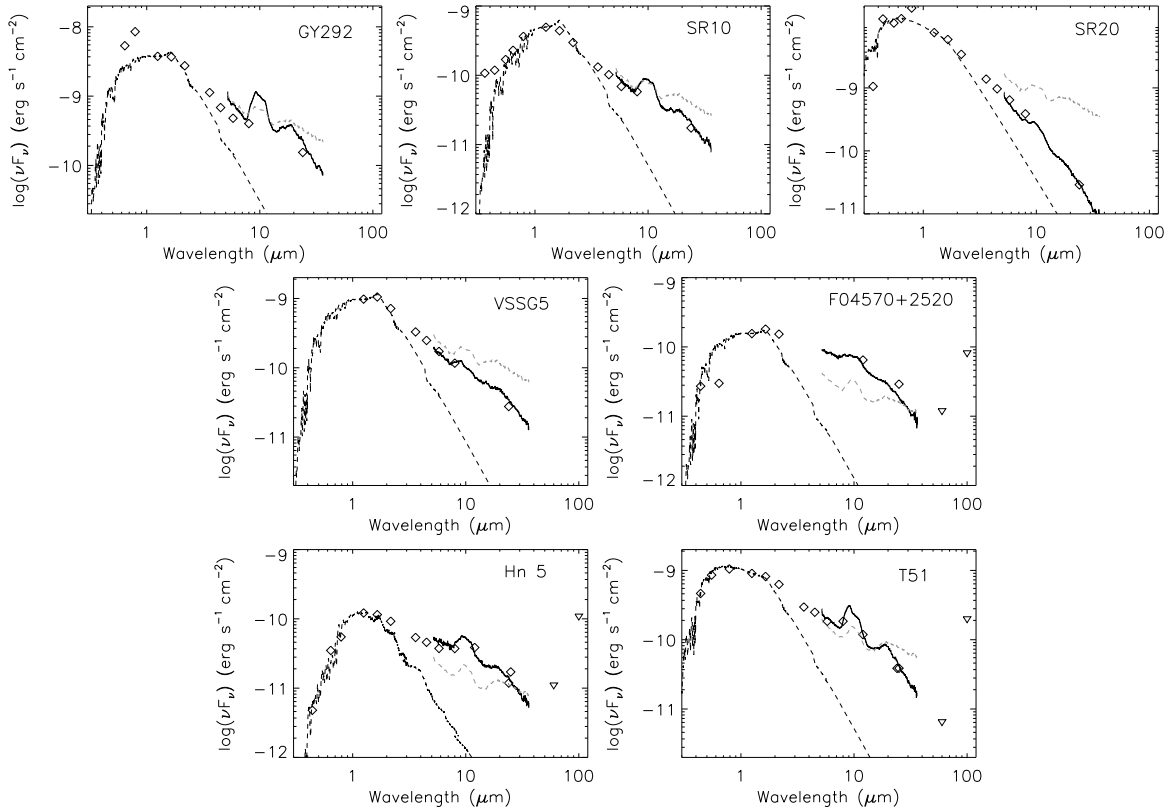


Fig. 17. | The dereddened SEDs of objects with very low n_{13-31} values ($< -4/3$); the photospheres are represented by Kurucz model atmospheres with solar metallicity, $\log(g)=3.5$, and different effective temperatures: $T_e = 4000$ K (GY292, F04570+2520), $T_e = 3625$ K (SR10), $T_e = 5500$ K (SR20), $T_e = 3875$ K (VSSG5), and $T_e = 4750$ K (T51). The photosphere for Hn 5 is an AMES-D dusty model atmosphere with $T_e = 3300$ K and $\log(g)=4.0$. The photometry was adopted from the literature, and the data were dereddened as explained in the text. The dashed gray lines represent the medians of the Ophiuchus core (for GY292, SR10, SR20, VSSG5), of Taurus (for F04570+2520), and of Chamaleon I (for Hn5 and T51), normalized at the H-band flux of each object.

inferred that a gap could be present in its disk. On the other hand, recent models suggest that the SED and mid-infrared visibilities of RY Tau can be reproduced with an accretion disk surrounded by an optically thin envelope, possibly replenished by a disk wind (Scheegerer et al. 2008).

LkCa 15, which is likely a single star (Leinert et al. 1993), has been recently modeled as a disk with a 46 AU inner hole that is not fully cleared out. An optically thick inner disk wall at the dust sublimation radius and an optically thin inner region extending out to a few AU were required to reproduce the near-infrared excess and 10 μ m silicate emission (Espaillat et al. 2007b,

2008). High-resolution interferometer images at millimeter wavelengths resolved the inner 50 AU hole of LkCa 15 in the dust continuum (Pietu et al. 2006), validating the SED model. It is possible that the other objects with an unusually large EW (10 μ m), decreased near- and mid-infrared excess, and steep SED rise beyond 15 μ m have such a disk gap filled with small, optically thin dust. In fact, Andrews et al. (2009) recently imaged an inner hole of 33 AU in the disk of ROX 44 using high-resolution sub-millimeter observations; they also note that, given that this object is still accreting and has a notable infrared excess, material must be present within the cavity detected in the millimeter continuum emission.

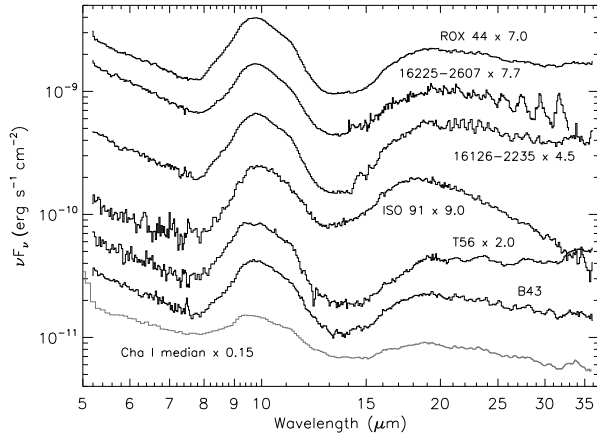


Fig. 18. | The most prominent outliers in terms of EW (10 μ m) in Chamaleon I and in the Ophiuchus σ -core region, compared to the median of Chamaleon I.

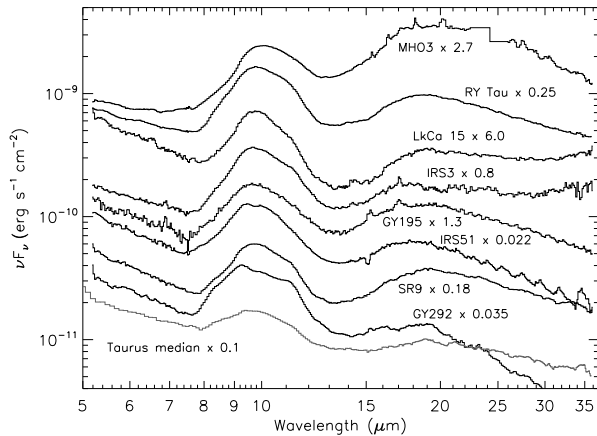


Fig. 19. | The most prominent outliers in terms of EW (10 μ m) in Taurus and in the Ophiuchus core region, compared to the median of Taurus.

The fraction of objects with unusually large EW (10 μ m), but typical n_{13-31} values, amounts to 30.7%, 21.5%, 19.5%, and 47.18% in the Ophiuchus core, Taurus, Chamaleon I, and Ophiuchus σ -core region, respectively. Thus, Ophiuchus has a marginally larger fraction of objects with an uncommon disk structure. Even though the Ophiuchus core suffers from larger extinction as compared to the other regions, we believe that the use of the MC Lure extinction curves for $A_V = 3$ does not overcorrect the 10 μ m silicate emission feature, and therefore our derived values of EW (10 μ m) are valid. Also, of the seven Ophiuchus σ -core outliers, only two have $A_V = 9$, and the four objects with the largest EW (10 μ m) values suffer from relatively little extinction.

5. DISCUSSION

5.1. First Steps of Disk Evolution

Circumstellar disks in the nearby star-forming regions of Ophiuchus, Taurus, and Chamaleon I display clear signs of disk evolution. When considering the spectral index between 13 and 31 μ m and the equivalent width of the 10 μ m silicate emission feature, outliers that do not fall in the region expected for typical accretion disks reveal altered, likely more evolved, disk structures. However, most of the objects have n_{13-31} and EW (10 μ m)

values that are not unusual (see Figures 10 to 13). When comparing them to model calculations, the fact that most disks have a negative spectral index suggests dust depletion factors of 10^2 to 10^3 in the upper disk layers, as was already found for Taurus (Furlan et al. 2006). Hardly any objects occupy the region where accretion disks with typical mass accretion rates of 10^9 to 10^8 $M_{\odot} \text{ yr}^{-1}$ and $\dot{M} = 1$ lie, even in the young Ophiuchus core, implying rapid dust growth and settling already at an age of ~ 1 Myr.

In previous work (e.g., Bouwman et al. 2001; van Boekel et al. 2003; Mees et al. 2003; Przygodda et al. 2003) the strength of the 10 μ m silicate feature was analyzed in a different way: it was estimated from the peak-over-continuum ratio in the 10 μ m region, and it was compared to the ux ratio of the normalized spectrum at 11.3 and 9.8 μ m, taken as a measure for the shape of the silicate feature. For both Herbig Ae/Be stars and T Tauri stars, a correlation between shape and strength is observed (e.g., van Boekel et al. 2003; Kessler-Silacci et al. 2006); strong features typically have low $F_{11.3}/F_{9.8}$ ratios, which is interpreted as emission from small, amorphous silicate grains, as are found in the interstellar medium. Conversely, a large $F_{11.3}/F_{9.8}$ ratio (and weak silicate feature strength) suggests the presence of larger and/or more crystalline grains, i.e., more processed dust.

Therefore, the large 10 μ m equivalent widths we observe in some of our spectra correspond to large peak-over-continuum ratios; they could be explained as objects with particularly large mass fractions of small grains in their disk surface layers. However, this interpretation does not take the optically thick disk component into account; if there were more small grains in the disk atmosphere absorbing stellar radiation, the lower disk layers would be heated more, resulting in an increase of continuum emission and no substantial change in the 10 μ m equivalent width. We checked this assumption by calculating new accretion disk models, which differ from the ones presented in x 4.1 only by the maximum grain size in the upper disk layers, 0.05 μ m as opposed to 0.25 μ m in the previous models. For these new models, the 10 μ m equivalent width increased by at most 0.2 μ m, proving that large EW (10 μ m) values cannot be explained by a large abundance of very small grains in the disk atmosphere. Also changing the dust composition does not significantly increase EW (10 μ m); we calculated models using opacities for amorphous silicates of olivine composition from Dorschner et al. (1995), which resulted in EW (10 μ m) values of up to 4 μ m for the less settled models (Espaillat 2009).

As noted by Watson et al. (2009), the interpretation of peak-over-continuum as different degrees of grain processing neglects the likely diversity in the structure of the underlying optically thick disk due to dust settling. A more settled disk will have decreased continuum emission and typically also less emission from the optically thin disk surface layers. Thus, our EW (10 μ m) values and also the peak-over-continuum ratios do not necessarily probe different grain sizes in the disk atmosphere, but rather are a measure for disk structure in terms of the ratio of the optically thin and optically thick emission.

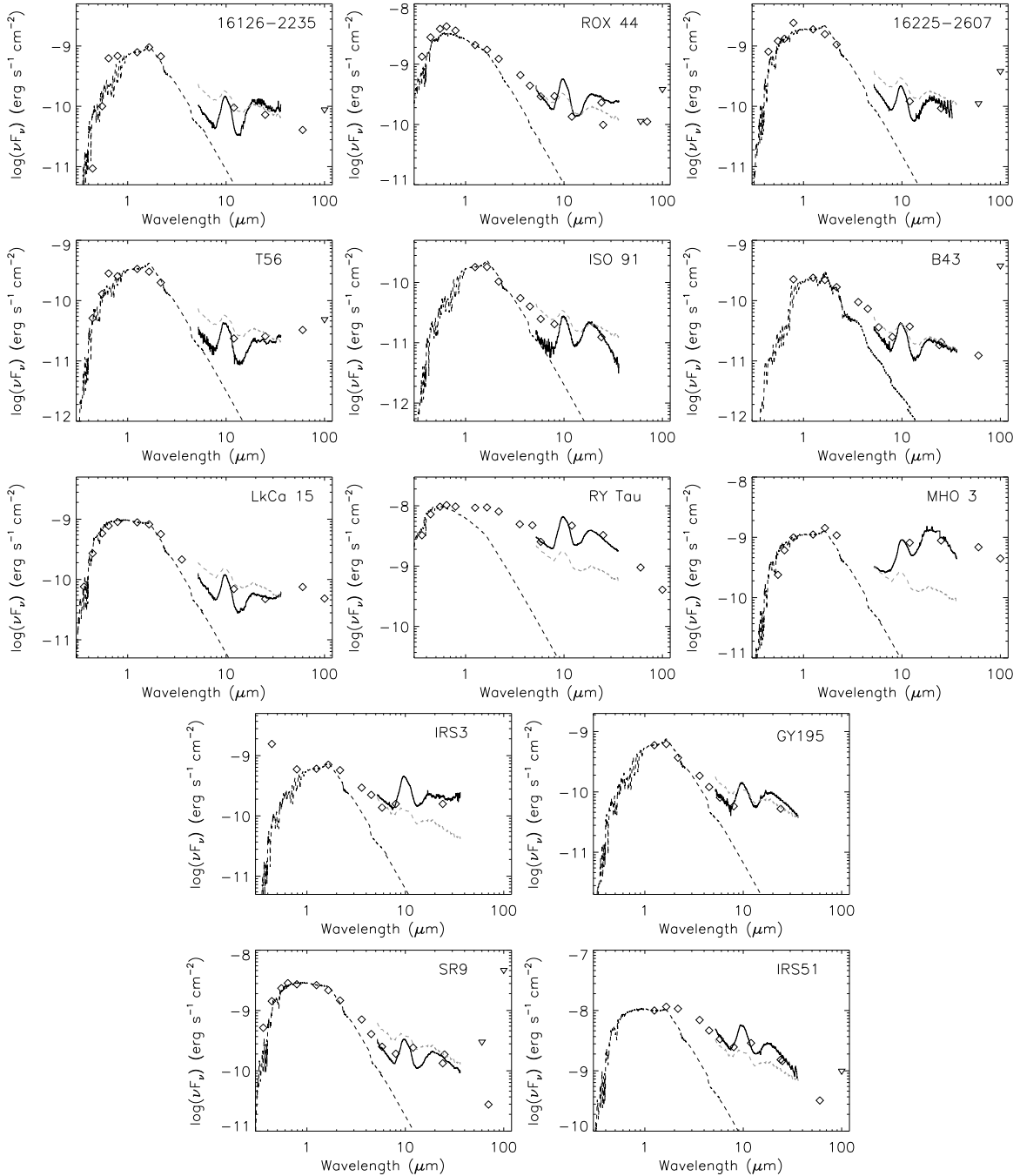


Fig. 20. The dereddened SEDs of objects with very prominent 10 μ m emission features; the SED of one additional object that also belongs to this category (GY 292) is shown in Figure 17. The photospheres for all objects except B 43 are represented by Kurucz model atmospheres with solar metallicity, $\log(g)=3.5$, and different effective temperatures: $T_e = 3500$ K (16126-2235, ISO 91, GY 195), $T_e = 5250$ K (ROX 44), $T_e = 4000$ K (16225-2607, MHO 3), $T_e = 3750$ K (T 56), $T_e = 4375$ K (LkCa 15, SR 9), $T_e = 6000$ K (RY Tau), $T_e = 3625$ K (IRS3), and $T_e = 4250$ K (IRS51). The photosphere for B43 is an AMES-D dusty model atmosphere with $T_e = 3500$ K and $\log(g)=3.5$. The photometry was adopted from the literature, and the data were dereddened as explained in the text. The dashed gray lines represent the medians of Chamaeleon I (16126-2235, ROX 44, 16225-2607, T 56, ISO 91, B43), of Taurus (LkCa 15, RY Tau, MHO 3), and of the Ophiuchus core (IRS3, GY 195, SR 9, IRS51), and normalized at the H-band flux of each object.

5.2. Formation of Disk Structure

The spectral index measures the degree of dust settling in a disk, but is also sensitive to disk inclination, especially for low mass accretion rates ($\sim 10^{-9}$ $M_{\odot} \text{ yr}^{-1}$). An n_{13-31} value larger than expected for a disk with no dust settling (i.e., $n = 1$) is indicative of a substantial change in the structure of the inner disk; all transitional disks studied so far in the Taurus and Chaeleon I regions have large n_{13-31} values and inner disk clearings ranging from a few to several tens of AU (D'Alessio et al. 2005; Calvet et al. 2005; Espaillat et al. 2007a,b; Kim et al. 2009).

Close binary companions create inner disk gaps whose size depends on the orbital parameters of the binary (Artymowicz & Lubow 1994). Such systems would appear as transitional disks, but in fact be long-lived circumbinary disks. The companion star fraction in the young star-forming regions of our study is fairly large,

50% (for projected separations in the 15-1800 AU range; Gehez et al. 1997), but it decreases for smaller separations of the binary components ($\sim 5\%$ for 0.02-0.5 AU projected separations; Meib 2003). More specifically, 40-50% of the stars in our sample are found in multiple systems, but not all objects have been observed at sufficiently high resolution to determine the presence of companions within $1''$. Thus, it is likely that a few of the transitional disks are the result of clearing by a central binary. In fact, CoKu Tau/4 and CS Cha have recently been found to be close binary systems (Ireland & Kraus 2008; Guenther et al. 2007), but it seems that only in CoKu Tau/4 are the stars responsible for inwardly truncating the disk.

On the other hand, disks are thought to evolve from inside out; processes occur on shorter timescales in the inner disk, where densities are higher and orbital speeds larger (e.g., Dullemond & Dominik 2004; Alexander & Armitage 2007). Substantial dust growth, planet formation, photoevaporation, or draining of the inner disk induced by the magneto-rotational instability (MRI) results in inner disk clearing (Marsh & Mahoney 1992; Clarke et al. 2001; D'Alessio et al. 2005; Alexander & Armitage 2007; Chiang & Murray-Clay 2007; Kim et al. 2009). If caused by these mechanisms of disk evolution, transitional disks are in a temporary state, since processes driving the clearing of the inner disk will eventually engulf the whole disk. The fact that we see evidence of inner disk clearing at the young age of L1688 (< 1 Myr) indicates that disk evolution starts early.

The frequency of transitional disks in the three main regions we studied (3-6% of objects at an age of 1-2 Myr) implies a timescale of several 10^4 up to 10^5 years for the transitional disk phase, assuming disk evolution is continuous and that all disks experience this stage in their evolution. It is also possible, but unlikely, that only 3-6% of disks in a star-forming region appear as transitional, with the mechanism that causes the inner disk hole active for a long period ($\sim 1-2$ Myr) of time, such as in a circumbinary disk. Disks are known to dissipate over time, with clearing processes on the timescale of $\sim 10^5$ years, as model calculations for disk clearing by planet formation (e.g., Quillen et al. 2004; Varniere et al. 2006), photoevaporation (e.g. Alexander et al. 2006), and MRI-

activated disk draining (Chiang & Murray-Clay 2007) have shown. The lifetime of a transitional disk is thus shorter than that of a primordial disk (a few Myr). Recent work by Currie & Kenyon (2009) suggests a long transitional disk timescale, but this is mainly due to the different definition of transitional disks; those authors consider all "evolved" disks as transitional, while we only include disks that show evidence of inner disk clearings. By adopting a similar definition of transitional disks as we do and using high-quality Spitzer data for Taurus and a consistent method of estimating disk fractions, Luhman et al. (2009) show that transition timescales appear to be considerably less than primordial disk lifetimes, substantiating our result.

The equivalent width of the $10 \mu\text{m}$ silicate emission feature could also suggest changes in the conformation of the disk, especially when accompanied by a decrease in the near- and mid-infrared emission. A large EW ($10 \mu\text{m}$) implies stronger emission by optically thin dust relative to the optically thick disk emission; a gap in the disk,

filled with optically thin dust, could create this signature and would be a precursor of a transitional disk with an inner disk hole (Espaillat et al. 2007b, 2008). On the other hand, an object with a dust-free gap would not exhibit a large EW ($10 \mu\text{m}$), as is the case for UX Tau A (Espaillat et al. 2007b). An alternative explanation for the EW ($10 \mu\text{m}$) outliers, as shown by modeling of RY Tau (Schegerer et al. 2008), is the presence of an envelope of optically thin dust that could be a source for the enhanced optically thin emission seen in these objects. However, this envelope would have to be replenished in small dust grains by some type of flows originating in the disk, and it is not known whether sufficiently high mass loss rates could be achieved.

Assuming most objects with large EW ($10 \mu\text{m}$) have developed gaps in their disks and that all disks experience this evolutionary phase once in their lifetime, the larger number of objects presumably with gaps in their disks compared to that of objects with inner holes ($\sim 20\%$ of objects at an age of 1-2 Myr) implies that the stage in which a disk has a gap lasts longer than the period of inner disk clearing, from several 10^5 up to 10^6 years. Alternatively, a disk with a gap could survive for a shorter period of time, but then experience this phase a few times before being dissipated. In addition, even if just a few of the disks with large EW ($10 \mu\text{m}$) in the Ophiuchus core were disks with gaps, the presence of such disks in this young region would suggest that gap formation sets in early. It is interesting that 50% of the objects in the Ophiuchus core region have unusually strong $10 \mu\text{m}$ emission features; if the gap interpretation holds true, it would be a region with a large fraction of evolved disks.

Of the disk clearing mechanisms mentioned above, planet formation is the most likely explanation for the existence of a gap between inner and outer optically thick disk regions. Photoevaporation and MRI-induced inner disk draining would not allow for a remnant inner, optically thick disk region (see also Espaillat et al. 2008), and it is unlikely that dust grain growth would be limited to a certain, well-defined radial range in the disk. Since a planet opening a gap will likely migrate inwards on roughly the viscous diffusion timescale of $\sim 10^4$ initial orbital periods (e.g., Lin & Papalizou 1986; Nelson et al.

2000), and the duration of the gap phase as estimated above could be at least a factor of a few larger, it is possible that in some systems we would be witnessing the effects of already the second or even later generation of planets. This type of scenario has also been proposed by Watson et al. (2009) to explain the variety of crystalline silicate abundances observed in T Tauri stars in Taurus. If we assume that at least some of the objects we studied have a disk gap opened by a planet, then these planets must have accumulated a mass of at least a few tens of Earth masses in ~ 1 Myr such that they are massive enough to open up gaps (see, e.g., Takeuchi et al. 1996). Gravitational instability can create massive planets on a timescale of $\sim 10^3$ years (e.g., Boss 2000), but also a migrating protoplanet can grow to a sufficiently large mass within $\sim 10^5$ years by accretion of planetesimals (Tanaka & Ida 1999).

A few objects with large n_{13-31} values also have large $10\ \mu\text{m}$ equivalent widths (e.g., DM Tau, GM Aur). The large spectral index suggests an inwardly truncated optically thick disk, with a disk wall at the inner radius. For cases where the presence of a near-infrared excess indicates that optically thin dust lies in the inner regions, the unusual strength of the $10\ \mu\text{m}$ feature can be explained by emission from this dust (see Calvet et al. 2005). On the other hand, for objects with no excess below about $8\ \mu\text{m}$ and therefore dust-depleted inner regions, the $10\ \mu\text{m}$ emission likely arises in the atmosphere of the wall (D'Alessio et al. 2005; Calvet et al. 2005). Thus, in a few cases, not only the object's location in n_{13-31} {EW ($10\ \mu\text{m}$)} space, but also the detailed shape of the SED are necessary to interpret disk structure.

5.3. Median Infrared Excess

The interpretation of disk evolution based on the median IRS spectrum is complicated by issues involving normalization. If the distribution of source fluxes in the near-IR and differences in the distances to the star-forming regions are taken into account, then the Class II objects in the Ophiuchus core, Taurus, and Cham aeleon I have very similar mid-infrared excess emission; the medians follow each other closely. This indicates that, on average, disk structures are similar and that comparable amounts of stellar radiation are reprocessed in the disk.

In particular, the Cham aeleon I star-forming region is very similar to Taurus in its disk evolution, as gauged from both the median IRS spectra of T Tauri stars and the fraction of objects with unusual 13–31 spectral slopes and $10\ \mu\text{m}$ equivalent widths. A green tint between these two regions is expected since their molecular cloud environments are comparable and their age difference is minimal, especially considering that there is an age spread in both regions (e.g., Palla & Stahler 2000), which might just be a result of observational uncertainties (Hartmann 2001).

Based on the distribution of near-IR fluxes, we found that the stars in Cham aeleon I are intrinsically fainter, while those in L1688 are brighter than their counterparts in Taurus. The latter observation can partly be explained by the somewhat higher fraction of earlier-type stars in our Ophiuchus sample as compared to the other two. In addition, since the Ophiuchus core region is younger than Taurus, we would expect more luminous young stars (e.g., Bara e et al. 2002). The age of 0.3–1 Myr for the

Ophiuchus core was derived assuming a distance of 165 pc (Luhman & Rieke 1999); the new distance determination of 120 pc by Loinard et al. (2008) implies that stars are a factor of 1.9 less luminous. Assuming they are contracting along Hayashi tracks at roughly constant effective temperature ($L / t^{2=3}$; Hartmann 1998), this would imply an increase in age by a factor of 2.6. Therefore, the median age of ~ 0.3 Myr found for Ophiuchus by Luhman & Rieke (1999) would change to ~ 0.8 Myr, making it just slightly younger than Taurus. The somewhat older age of Cham aeleon I, as compared to the other regions, could explain the reduced luminosity of its stars.

The shape of the median $10\ \mu\text{m}$ silicate emission feature in the three regions suggests that the disks in L1688 and Cham aeleon I might have, on average, more crystalline silicates than those in Taurus. Since some processing at high temperatures is required to transform the amorphous silicate grains from the interstellar medium into crystalline form (e.g., Harker & Desch 2002), we would expect an older star-forming region, which had more time for this processing to take place, to have a larger fraction of crystalline grains. On the other hand, the larger degree of dust processing in the youngest region of our sample, L1688, could be a result of different initial conditions in the dense Ophiuchus core region. If the mass accretion rates or the masses of the disks were higher, disks would likely evolve faster. This could also explain the large fraction of settled disks (those with $n_{13-31} < 0$) in L1688, which is basically the same as in the slightly older Taurus region. The fact that our Ophiuchus core sample seems to be biased towards somewhat more massive, young stars supports the idea of faster disk evolution, given that there are indications that intermediate-mass stars evolve faster than low-mass stars (Hernandez et al. 2005).

6. CONCLUSIONS

We analyzed the IRS spectra of Class II objects in the Ophiuchus core, Ophiuchus α -core, Taurus, and Cham aeleon I star-forming regions. Our main conclusions are as follows:

The spectral index between 13 and $31\ \mu\text{m}$, n_{13-31} , and the equivalent width of the $10\ \mu\text{m}$ silicate emission feature, EW ($10\ \mu\text{m}$), are useful indicators for the degree of disk evolution. We interpret Class II objects with unusually large n_{13-31} as transitional disks with inner disk clearings, while objects with very substantial EW ($10\ \mu\text{m}$) and decreased near- and mid-infrared excess emission could have gaps in their disks that are filled with optically thin dust (see also Espaillat et al. 2007b). Considering various disk clearing mechanisms, the most likely explanation for gaps within optically thick disks is planet formation.

The Ophiuchus α -core region, which is of similar age as Cham aeleon I (~ 2 Myr), has a marginally larger fraction of Class II objects whose n_{13-31} and EW ($10\ \mu\text{m}$) are outside the range found for typical accretion disks, as compared to the other three regions. However, the sample size is small, and therefore, if these outliers are interpreted as objects with an evolved disk structure, we can only tentatively conclude that the Ophiuchus α -core is the most evolved region.

The transitional disk fraction amounts to a few % in all four regions; while L1688 lacks any disks with inner

TABLE 5
Target names and coordinates

Name	R.A. (J2000)	Dec. (J2000)
04108+2910	04 13 57.38	29 18 19.3
04187+1927	04 21 43.24	19 34 13.3
04200+2759	04 23 07.77	28 05 57.3
04216+2603	04 24 44.58	26 10 14.1
04303+2240	04 33 19.07	22 46 34.2

Note. | Table 5 is published in its entirety in the electronic edition of the *Astronomical Journal*. A portion is shown here for guidance regarding its form and content.

regions fully depleted in small dust grains, the frequency of transitional disks in Chamæleon I is comparable to that of the Taurus region. Assuming disk evolution is continuous and affects the structure of the inner disk at some point in the lifetime of a disk, we infer that the transitional disk phase lasts for several 10^4 up to 10^5 years.

The shape and normalized flux levels of the median mid-infrared spectrum of disks in Taurus and Chamæleon I are very similar, and the fractions of objects with unusually large EW (10 μ m), but typical n_{13-31} values, are essentially the same. This suggests that the similar star-forming environments and age ranges of these two regions result in an overall comparable degree of disk evolution.

The median mid-infrared excess of T Tauri stars in the Ophiuchus core region is also similar to that in Taurus and Chamæleon I. The shape of the median 10 μ m silicate emission feature hints at the presence of larger grains and crystalline silicates, and therefore dust grains already experienced some processing. This region also has a sizable fraction ($\sim 30\%$) of Class II objects with large 10 μ m equivalent widths, which could indicate that disk evolution sets in early.

We are likely witnessing the combined effect of age and molecular cloud environment on disk evolution. The inner disks in the Taurus, Chamæleon I, and Ophiuchus α -core regions, but also in the younger and denser Ophiuchus core, show clear signs of evolution, like the presence of larger grains and decreased α -ring, indicative of dust sedimentation. Some disks also display evidence for structure formation, like the development of inner holes and possibly also gaps. This suggests that grain growth, settling, and crystallization occur fast, but the development of radial structure in a disk requires, on average, more time and might be a transient phenomenon. Our

analysis implies that the degree of disk evolution does not necessarily correlate with age during the first few million years, since it sets in relatively early, and the subsequent evolution might be dictated more by the individual system properties than some universal processes happening at set time intervals.

We thank the referee for a thoughtful review that led us to improve this paper. This work is based on observations made with the Spitzer Space Telescope, which is operated by the Jet Propulsion Laboratory (JPL), California Institute of Technology (Caltech), under NASA contract 1407. Support for this work was provided by NASA through contract number 1257184 issued by JPL/Caltech. E.F. was partly supported by a NASA Postdoctoral Program Fellowship, administered by Oak Ridge Associated Universities through a contract with NASA, and partly supported by NASA through the Spitzer Space Telescope Fellowship Program, through a contract issued by JPL/Caltech under a contract with NASA. N.C. and L.H. acknowledge support from NASA Origins grants NNG 05G 126G, NNG 06G J32G, and NNX 08AH 94G. P.D. acknowledges grants from CONACYT, Mexico. This publication makes use of data products from the Two Micron All Sky Survey, which is a joint project of the University of Massachusetts and the Infrared Processing and Analysis Center/Caltech, funded by NASA and the NSF. It has also made use of the SIMBAD and VizieR databases, operated at CDS (Strasbourg, France), NASA's Astrophysics Data System Abstract Service, and of the NASA/IPAC Infrared Science Archive operated by JPL, Caltech, under contract with NASA.

Facilities: Spitzer (IRS)

APPENDIX

Additional tables are provided in the electronic edition. To show their format and content type, the first few lines of these tables are printed here. Table 5 contains the target names and coordinates of our sample of Class II objects in Taurus, Chamæleon I, and the Ophiuchus core and α -core regions. Table 6 contains the median IRS spectra and their lower and upper quartiles for the Ophiuchus core, Chamæleon I, and Taurus regions, normalized at the 2MASS H-band fluxes. Here, only the first few entries of the Ophiuchus core median and quartiles are shown. These are the medians displayed in Figure 3 as solid lines.

TABLE 6
Ophiuchus core median (H normalization)

(m)	F (erg/s/cm ²)	F _{lower} (erg/s/cm ²)	F _{upper} (erg/s/cm ²)
5.0	4.960E-10	3.300E-10	7.499E-10
5.1	4.561E-10	2.778E-10	7.436E-10
5.2	4.002E-10	2.350E-10	5.905E-10
5.3	3.665E-10	2.123E-10	5.743E-10
5.4	3.509E-10	2.043E-10	5.385E-10
5.5	3.241E-10	1.907E-10	4.998E-10

Note. | Table 6 is published in its entirety in the electronic edition of the Astrophysical Journal. A portion is shown here for guidance regarding its form and content.

REFERENCES

- Adams, F. C., Lada, C. H., & Shu, F. H. 1987, *ApJ*, 312, 788
- Alexander, R. D., Clarke, C. J., & Pringle, J. E. 2006, *MNRAS*, 369, 229
- Alexander, R. D., & Armitage, P. J. 2007, *MNRAS*, 375, 500
- Andre, P., & Montmerle, T. 1994, *ApJ*, 420, 837
- Andrews, S. M., Wilner, D. J., Hughes, A. M., Qi, C., & Dullemond, C. P. 2009, *ApJ*, in press, arXiv:0906.0730 [astro-ph]
- Apai, D., Pascucci, I., Bouwman, J., Natta, A., Henning, Th., & Dullemond, C. 2005, *Science*, 310, 834
- Artyomowicz, P., & Lubow, S. H. 1994, *ApJ*, 421, 651
- Baran, E., Chabrier, G., Allard, F., & Hauschildt, P. H. 2002, *A & A*, 382, 563
- Barsony, M., Kenyon, S. J., Lada, E. A., & Teuben, P. J. 1997, *ApJS*, 112, 109
- Bertout, C., Robichon, N., & Arénaud, F. 1999, *A & A*, 352, 574
- Bontemps, S., André, P., Kulas, A. A., Nordh, L., Olsson, G., Hultgren, M., Abergel, A., Błomqvist, J., et al. 2001, *A & A*, 372, 173
- Boss, A. P. 2000, *ApJ*, 536, L101
- Bouwman, J., Meus, G., de Koter, A., Hony, S., Dominik, C., & Waters, L. B. F. M. 2001, *A & A*, 375, 950
- Brandner, W., & Zinnecker, H. 1997, *A & A*, 321, 220
- Briceno, C., Hartmann, L., Staufer, J., & Martín, E. 1998, *AJ*, 115, 2074
- Briceno, C., Luhman, K. L., Hartmann, L., Staufer, J. R., & Kirkpatrick, J. D. 2002, *ApJ*, 580, 317
- Brown, J. M., Blake, G. A., Dullemond, C. P., Merín, B., Augereau, J. C., Boogert, A. C. A., Evans, N. J., Geers, V. C., et al. 2007, *ApJ*, 664, L107
- Calvet, N., Muzerolle, J., Briceno, C., Hernandez, J., Hartmann, L., Saucedo, J. L., & Gordon, K. D. 2004, *AJ*, 128, 1294
- Calvet, N., D'Alessio, P., Watson, D. M., Franco-Hernandez, R., Furlan, E., Green, J., Sutter, P. M., Forrest, W. J., et al. 2005, *ApJ*, 630, L185
- Cambrésy, L., Copet, E., Epchtein, N., de Batz, B., Borsenberger, J., Fouque, P., Kimeswenger, S., & Tiphène, D. 1998, *A & A*, 338, 977
- Cardelli, J. A., Clayton, G. C., & Mathis, J. S. 1989, *ApJ*, 345, 245
- Chen, H., Myers, P. C., Ladd, E. F., & Wood, D. O. S. 1995, *ApJ*, 445, 377
- Chen, H., Grenfell, T. G., Myers, P. C., & Hughes, J. D. 1997, *ApJ*, 478, 295
- Chiang, E. I., & Goldreich, P. 1997, *ApJ*, 490, 368
- Chiang, E., & Murray-Clay, R. 2007, *Nature Physics*, 3, 604
- Chiar, J. E., Ennico, K., Pendleton, Y. J., Boogert, A. C. A., Greene, T., Knez, C., Lada, C., Roellig, et al. 2007, *ApJ*, 666, L73
- Clarke, C. J., Gendrin, A., & Sotomayor, M. 2001, *MNRAS*, 328, 485
- Cohen, M., & Kuhl, L. V. 1979, *ApJS*, 41, 743
- Correia, S., Zinnecker, H., Ratzka, Th., & Sterzik, M. F. 2006, *A & A*, 459, 909
- Currie, T., & Kenyon, S. J. 2009, *AJ*, 138, 703
- D'Alessio, P., Calvet, N., Hartmann, L., Lizano, S., & Canto, J. 1999, *ApJ*, 527, 893
- D'Alessio, P., Hartmann, L., Calvet, N., Franco-Hernandez, R., Forrest, W. J., Sargent, B., Furlan, E., Uchida, K., et al. 2005, *ApJ*, 621, 461
- D'Alessio, P., Calvet, N., Hartmann, L., Franco-Hernandez, R., & Servén, H. 2006, *ApJ*, 638, 314
- Dorschner, J., Begemann, B., Henning, Th., Jäger, C., & Mutschke, H. 1995, *A & A*, 300, 503
- Doucet, C., Habart, E., Pantin, E., Dullemond, C., Lagage, P. O., Pinte, C., Duchêne, G., & Ménard, F. 2007, *A & A*, 470, 625
- Draine, B. T., & Lee, H. M. 1984, *ApJ*, 285, 89
- Duchêne, G., Ghez, A. M., McCabe, C., & Weinberger, A. J. 2003, *ApJ*, 592, 288
- Dullemond, C. P., & Dominik, C. 2004, *A & A*, 421, 1075
- Dullemond, C. P., & Dominik, C. 2005, *A & A*, 434, 971
- Espaillet, C., Calvet, N., D'Alessio, P., Bergin, E., Hartmann, L., Watson, D. M., Furlan, E., Najita, N., et al. 2007a, *ApJ*, 664, L111
- Espaillet, C., Calvet, N., D'Alessio, P., Hernandez, J., Qi, C., Hartmann, L., Furlan, E., & Watson, D. M. 2007b, *ApJ*, 670, L135
- Espaillet, C., Calvet, N., Luhman, K. L., Muzerolle, J., & D'Alessio, P. 2008, *ApJ*, 682, L125
- Espaillet, C. 2009, Ph.D. thesis, University of Michigan
- Fabian, D., Henning, Th., Jäger, C., Mutschke, H., Dorschner, J., & Wehrhan, O. 2001, *A & A*, 378, 228
- Feigelson, E. D., & Kriss, G. A. 1989, *ApJ*, 338, 262
- Forrest, W. J., et al. 2004, *ApJS*, 154, 443
- Furlan, E., Calvet, N., D'Alessio, P., Hartmann, L., Forrest, W. J., Watson, D. M., Uchida, K. I., Sargent, B., et al. 2005, *ApJ*, 628, L65
- Furlan, E., Hartmann, L., Calvet, N., D'Alessio, P., Franco-Hernandez, R., Forrest, W. J., Watson, D. M., Uchida, K. I., et al. 2006, *ApJS*, 165, 568
- Gauvin, L. S., & Strom, K. M. 1992, *ApJ*, 385, 217
- Geers, V. C., Augereau, J.-C., Pontoppidan, K. M., Dullemond, C. P., Visser, R., Kessler-Silacci, J. E., Evans, N. J., van Dishoeck, E. F., et al. 2006, *A & A*, 459, 545
- Geers, V. C., Pontoppidan, K. M., van Dishoeck, E. F., Dullemond, C. P., Augereau, J.-C., Merín, B., Oliveira, I., & Pel, J. W. 2007, *A & A*, 469, L35
- Ghez, A. M., Neugebauer, G., & Matthews, K. 1993, *AJ*, 106, 2005
- Ghez, A. M., Weinberger, A. J., Neugebauer, G., Matthews, K., & McCarthy, D. W. 1995, *AJ*, 110, 753
- Ghez, A. M., McCarthy, D. W., Patience, J. L., & Beck, T. L. 1997, *ApJ*, 481, 378
- Goldreich, P., & Ward, W. R. 1973, *ApJ*, 183, 1051
- Gomez, M., & Mardones, D. 2003, *AJ*, 125, 2134
- Greene, Th. P., & Young, E. T. 1992, *ApJ*, 395, 516
- Greene, Th. P., Wilking, B. A., André, P., Young, E. T., & Lada, C. H. 1994, *ApJ*, 434, 614
- Guenther, E. W., Esposito, M., Mundt, R., Covino, E., Alcalá, J. M., Cusano, F., & Stecklum, B. 2007, *A & A*, 467, 1147
- Haisch, K. E., Lada, E. A., & Lada, C. H. 2001, *ApJ*, 553, L153
- Harker, D. E., & Desch, S. J. 2002, *ApJ*, 565, L109
- Hartigan, P., Strom, K. M., & Strom, S. E. 1994, *ApJ*, 427, 961
- Hartigan, P., & Kenyon, S. J. 2003, *ApJ*, 583, 334
- Hartmann, L. 1998, *Accretion Processes in Star Formation* (Cambridge: Cambridge University Press)
- Hartmann, L., Calvet, N., Gullbring, E., & D'Alessio, P. 1998, *ApJ*, 495, 385
- Hartmann, L. 2001, *AJ*, 121, 1030
- Hebig, G. H., & Bell, K. R. 1988, *Lick Observatory Bulletin*, Santa Cruz: Lick Observatory, 1988
- Hernandez, J., Calvet, N., Hartmann, L., Briceno, C., Sicilia-Aguilar, A., & Berlind, P. 2005, *AJ*, 129, 856
- Hernandez, J., Briceno, C., Calvet, N., Hartmann, L., Muzerolle, J., & Quintero, A. 2006, *ApJ*, 652, 472
- Higdon, S. J. U., et al. 2004, *PASP*, 116, 975
- Hillenbrand, L. A., Strom, S. E., Viba, F., & Keene, J. 1992, *ApJ*, 397, 613
- Houck, J. R., et al. 2004, *ApJS*, 154, 18
- Hughes, A. M., Andrews, S. M., Espaillet, C., Wilner, D. J., Calvet, N., D'Alessio, P., Qi, C., Williams, J. P., & Hogerheijde, M. R. 2009, *ApJ*, 698, 131
- Ichikawa, T., & Nishida, M. 1989, *AJ*, 97, 1074
- Ireland, M. J., & Kaus, A. L. 2008, *ApJ*, 678, L59
- Jäger, C., Molster, F. J., Dorschner, J., Henning, Th., Mutschke, H., Waters, L. B. F. M. 1998, *A & A*, 339, 904
- Jayawardhana, R., Hartmann, L., Fazio, G., Fisher, R. S., Telesco, C. M., & Pina, R. K. 1999, *ApJ*, 521, L129
- Jayawardhana, R., Coey, J., Scholz, A., Brandeker, A., & van Kerckwijk, M. H. 2006, *ApJ*, 648, 1206
- Jensen, E. L. N., Mathieu, R. D., Donar, A. X., & Dullaghan, A. 2004, *ApJ*, 600, 789
- Kenyon, S. J., Hartmann, L. W., Strom, K. M., & Strom, S. E. 1990, *AJ*, 99, 869
- Kenyon, S. J., & Hartmann, L. 1995, *ApJS*, 101, 117
- Kenyon, S. J., Brown, D. I., Tout, Ch. A., & Berlind, P. 1998, *AJ*, 115, 2491

- Kessler-Silacci, J., Augereau, J.-C., Dullemond, C. P., Geers, V., Lahuis, F., Evans, N. J., van Dishoeck, E. F., Blake, G. A., et al. 2006, *ApJ*, 639, 275
- Kim, K. H., Watson, D. M., Manoj, P., Furlan, E., Najita, J., Forrest, W. J., Sargent, B., Espaillat, C., et al. 2009, *ApJ*, 700, 1017
- Lada, C. J. 1987, in *Star Forming Regions*, proceedings of the IAU Symposium No. 115, ed. M. Peimbert & J. Jugaku, Dordrecht: Reidel, 1
- Lafreniere, D., Jayawardhana, R., Brandeker, A., Ahmic, M., & van Kerkwijk, M. H. 2008, *ApJ*, 683, 844
- Leinert, Ch., Zinnecker, H., Weitzel, N., Christou, J., Ridgway, S. T., Jameson, R., Haas, M., & Lenzen, R. 1993, *A & A*, 278, 129
- Lin, D. N. C., & Pappalizou, J. 1986, *ApJ*, 309, 846
- Lin, D. N. C., Pappalizou, J. C. B., Terquem, C., Bryden, G., & Ida, S. 2000, in *Protostars and Planets IV*, eds. V. Mannings, A. P. Boss, & S. S. Russell (Tucson: Univ. Arizona Press), 1111
- Loinard, L., Torres, R. M., Mioduszewski, A., & Rodriguez, L. F. 2008, *ApJ*, 675, L29
- Loren, R. B. 1989, *ApJ*, 338, 902
- Luhman, K. L. 2000, *ApJ*, 544, 1044
- Luhman, K. L. 2004a, *ApJ*, 602, 816
- Luhman, K. L. 2004b, *ApJ*, 617, 1216
- Luhman, K. L. 2007, *ApJS*, 173, 104
- Luhman, K. L., & Rieke, G. H. 1999, *ApJ*, 525, 440
- Luhman, K. L., Staufer, J. R., Muench, A. A., Rieke, G. H., Lada, E. A., Bouvier, J., & Lada, C. J. 2003, *ApJ*, 593, 1093
- Luhman, K. L., Allen, P. R., Espaillat, C., Hartmann, L., & Calvet, N. 2009, *ApJ*, submitted
- Marsh, K. A., & Mahoney, M. J. 1992, *ApJ*, 395, L115
- Martin, E. L., Mouton, T., Gregorio-Hetem, J., & Casanova, S. 1998, *MNRAS*, 300, 733
- Mathis, J. S. 1990, *ARA & A*, 28, 37
- McClure, M. K., Forrest, W. J., Sargent, B. A., Watson, D. M., Furlan, E., Manoj, P., Luhman, K. L., Calvet, N., et al. 2008, *ApJ*, 683, L187
- McClure, M. K. 2009, *ApJ*, 639, L81
- Meus, G., Sterzik, M., Bouwman, J., & Natta, A. 2003, *A & A*, 409, L25
- Melo, C. H. F. 2003, *A & A*, 410, 269
- Meyer, M. R., Calvet, N., & Hillenbrand, L. A. 1997, *AJ*, 114, 288
- Miyake, K., & Nakagawa, Y. 1995, *ApJ*, 441, 361
- Natta, A., Testi, L., & Randich, S. 2006, *A & A*, 452, 245
- Nelson, R. P., Pappalizou, J. C. B., Masset, F., & Key, W. 2000, *MNRAS*, 318, 18
- Padgett, D. L., Rebull, L. M., Stapelfeldt, K. R., Chapman, N. L., Lai, S.-P., Mundy, L. G., Evans, N. J., Brooke, T. Y., et al. 2008, *ApJ*, 672, 1013
- Palla, F., & Stahler, S. W. 2000, *ApJ*, 540, 255
- Persi, P., Marzani, A. R., Olofsson, G., Kaa, A. A., Nordh, L., Hultgren, M., Abergel, A., Andre, P., et al. 2000, *A & A*, 357, 219
- Pietu, V., Dutrey, A., Guilloteau, S., Chapillon, E., & Pety, J. 2006, *A & A*, 460, L43
- Rato, L., Greene, T. P., & Simon, M. 2003, *ApJ*, 584, 853
- Reibisch, Th., Guenther, E., Zinnecker, H., Sterzik, M., Frink, S., & Roser, S. 1998, *A & A*, 333, 619
- Rzygodda, F., van Boekel, R., Abraham, P., Melnikov, S. Y., Waters, L. B. F. M., & Leinert, Ch. 2003, *A & A*, 412, L43
- Quillen, A. C., Blackman, E. G., Frank, A., & Vamieri, P. 2004, *ApJ*, 612, L137
- Ratzka, T., Kohler, R., & Leinert, Ch. 2005, *A & A*, 437, 611
- Reipurth, B., & Zinnecker, H. 1993, *A & A*, 278, 81
- Sargent, B., Forrest, W. J., D'Alessio, P., Li, A., Najita, J., Watson, D. M., Calvet, N., Furlan, E., et al. 2006, *ApJ*, 645, 395
- Sargent, B. A., Forrest, W. J., Tayrien, C., McClure, M. K., Watson, D. M., Sloan, G. C., Li, A., Manoj, P., et al. 2009, *ApJS*, 182, 477
- Scheigerer, A. A., Wolf, S., Ratzka, Th., & Leinert, Ch. 2008, *A & A*, 478, 779
- Sicilia-Aguilar, A., Hartmann, L., Calvet, N., Meeath, S. T., Muzerolle, J., Allen, L., D'Alessio, P., Merin, B., et al. 2006, *ApJ*, 638, 897
- Simon, M., Ghez, A. M., Leinert, Ch., Cassar, L., Chen, W. P., Howell, R. R., Jameson, R. F., Matthews, K., Neugebauer, G., & Richichi, A. 1995, *ApJ*, 443, 625
- Skrutskie, M. F., Dutkevitch, D., Strom, S. E., Edwards, S., & Strom, K. M. 1990, *AJ*, 99, 1187
- Skrutskie, M. F., et al. 2006, *AJ*, 131, 1163
- Strom, K. M., & Strom, S. E. 1994, *ApJ*, 424, 237
- Takeuchi, T., Miyama, S. M., & Lin, D. N. C. 1996, *ApJ*, 460, 832
- Tanaka, H., & Ida, S. 1999, *Icarus*, 139, 350
- Torres, C. A. O., Quast, G., de la Reza, R., Gregorio-Hetem, J., & Lepine, J. R. D. 1995, *AJ*, 109, 2146
- Torres, C. A. O., Quast, G. R., da Silva, L., de la Reza, R., Melo, C. H. F., & Sterzik, M. 2006, *A & A*, 460, 695
- Torres, R. M., Loinard, L., Mioduszewski, A. J., & Rodriguez, L. F. 2007, *ApJ*, 671, 1813
- van Boekel, R., Waters, L. B. F. M., Dominik, C., Bouwman, J., de Koter, A., Dullemond, C. P., & Paresce, F. 2003, *A & A*, 400, L21
- Vamieri, P., Blackman, E. G., Frank, A., & Quillen, A. C. 2006, *ApJ*, 640, 1110
- Vieira, S. L. A., Corradi, W. J. B., Alencar, S. H. P., Mendes, L. T. S., Torres, C. A. O., Quast, G. R., Guimarães, M. M., & da Silva, L. 2003, *AJ*, 126, 2971
- Watson, D. M., Leisenring, J. M., Furlan, E., Bohac, C. J., Sargent, B., Forrest, W. J., Calvet, N., Hartmann, L., et al. 2009, *ApJS*, 180, 84
- Wenrich, M. L., & Christensen, P. R. 1996, *J. Geophys. Res.*, 101, 15921
- Werner, M. W. et al. 2004, *ApJS*, 154, 1
- White, R. J., & Basri, G. 2003, *ApJ*, 582, 1109
- White, R. J., & Ghez, A. M. 2001, *ApJ*, 556, 265
- White, R. J., & Hillenbrand, L. A. 2004, *ApJ*, 616, 998
- Whittet, D. C. B., Pustni, T., Franco, G. A. P., Gerakines, P. A., Kilkenny, D., Larson, K. A., & Wesselius, P. R. 1997, *A & A*, 327, 1194
- Whittet, D. C. B., Bode, M. F., Longmore, A. J., Adamson, A. J., McFadzean, A. D., Atken, D. K., & Roche, P. F. 1988, *MNRAS*, 233, 321
- Whittet, D. C. B., Shenoy, S. S., Clayton, G. C., & Gordon, K. D. 2004, *ApJ*, 602, 291
- Wilking, B. A., Lada, C. J., & Young, E. T. 1989, *ApJ*, 340, 823
- Wilking, B. A., Meyer, M. R., Robinson, J. G., & Greene, T. H. P. 2005, *AJ*, 130, 1733

TABLE 1
Properties of the targets in the Ophiuchus core region

Name (1)	Spectral Type ^a (2)	A_V ^b (3)	EW (10 μ m) (4)	n_{13-31} (5)	Median (6)
16220-2452	M 3	3.7	4.87	-0.09	
16237-2349	K 5.5	5.0	1.67	-0.17	
B162713-241818	M 0	13.0	1.39	-1.28	
DoAr24	K 5	4.1	3.78	-0.39	
GSS29	M 1	11.5	2.65	-1.15	
GSS31	G 6	7.0	1.58	-0.50	
GSS37	M 0	8.7	1.47	-1.23	
GSS39	M 0	17.2	1.15	-0.75	
GY 144	M 5	40.3	3.23	-0.86	
GY 154	M 6	23.3	2.63	-0.27	
GY 188	M 3	40.7	1.85	0.15	
GY 195	M 3	24.7	6.23	-0.15	
GY 204	M 5.5	3.4	3.41	0.22	
GY 213	M 4	27.3	3.21	-0.95	
GY 224	M 4	34.2	3.94	-0.49	
GY 235	M 5	8.7	3.02	0.14	
GY 245		44.2	3.53	-0.72	
GY 260	M 4	31.7	2.31	-0.18	
GY 284	M 3.25	7.0	3.60	0.08	
GY 289	M 2	24.0	1.54	-0.20	
GY 292	K 7	13.5	6.31	-1.41	
GY 301	K 7	40.4	3.15	-0.26	
GY 310	M 4	7.5	2.92	0.31	
GY 314	K 5	8.1	1.08	-0.20	
GY 323	M 5	32.8	2.99	-1.17	
GY 326	M 2	10.2	2.44	-0.48	
GY 344	M 6	19.1	1.35	0.02	
GY 350	M 6	8.5	2.53	-0.94	
GY 352	M 5	20.3	0.91	-1.10	
GY 371	M 6	6.3	0.44	-0.71	
GY 397	M 6	5.8	1.18	-0.76	
HD 147889	B 2	4.4	0.02	-0.11	
IRS 2	K 3.5	7.7	1.53	-0.23	
IRS 26	M 6	19.6	3.41	-0.78	
IRS 3	M 2	8.5	6.56	0.37	
IRS 33	M 2	40.5	0.99	-1.08	
IRS 34	M 0	28.7	0.85	-0.94	
IRS 35		45.7	3.65	-1.03	
IRS 42	K 7	29.0	3.08	-0.90	
IRS 45	K 6.5	24.5	1.59	-0.87	
IRS 47	M 3	28.0	1.66	-1.33	
IRS 48	A 0	15.0	-0.30	1.33	
IRS 49	K 5	12.2	3.67	-0.11	
IRS 51	K 6	37.6	5.53	-0.64	
S 2	M 0	11.8	0.55	-1.33	
SR 4	K 4.5	2.6	2.29	0.29	
SR 9	K 5	1.9	5.87	0.02	
SR 10	M 2	1.5	3.03	-1.34	
SR 20	G 7	7.0	1.21	-2.53	
SR 21	F 4	8.0	4.01	1.57	
VSS 27	G 3.5	8.1	1.53	-0.97	
VSSG 1	M 0	16.5	0.88	-1.25	
VSSG 5	M 0	20.3	1.00	-1.46	
VSSG 25	M 4	13.6	3.38	-0.21	
W L 1	M 4	28.2	4.51	-0.19	
W L 2	M 0	34.8	2.63	-0.68	
W L 3	M 4	42.0	1.34	-0.42	
W L 4	M 1.5	21.3	1.77	0.06	
W L 10	K 7	13.3	1.08	-0.31	
W L 11	M 0	15.9	1.97	-0.41	
W L 18	K 6.5	12.2	1.40	-0.34	
W SB 37	M 5	2.9	1.23	-0.88	
W SB 60	M 4.5	4.5	2.01	0.05	

Note. | Column (1) lists the name of the object, column (2) the adopted spectral type, column (3) the optical extinction A_V (assuming $R_V = 3.1$), column (4) the 10 μ m equivalent width (EW (10 μ m)), column (5) the 13–31 μ m spectral index (n_{13-31}), and the \square symbol in column (6) indicates that the object was used in the median calculation. Note that uncertainties in A_V , ranging from 1% to 30% of the A_V value (MCClure et al., in preparation), account for \sim 25% of the error bars of EW (10 μ m) and n_{13-31} .

^a Spectral types were taken from Brandner & Zinnecker (1997); Luhman & Rieke (1999); Wilking et al. (2005); Natta et al. (2006); MCClure et al. (in preparation).

^b A_V values are from MCClure et al. (in preparation).

TABLE 2
Properties of the targets in the Taurus region

Name (1)	Spectral Type ^a (2)	A_V ^a (3)	EW (10 m) (4)	n_{13-31} (5)	Median (6)
04108+ 2910	M 0	1.4	0.28	-0.79	
04187+ 1927	M 0	0.0	0.94	-0.84	
04200+ 2759		0.0	1.52	-0.41	
04216+ 2603	M 1	0.0	1.16	-0.41	
04303+ 2240		11.7	2.21	-1.15	
04370+ 2559		9.8	4.06	-0.51	
04385+ 2550	M 0	7.8	2.48	0.26	
AA Tau	K 7	1.8	1.79	-0.51	
AB Aur	A 0	0.3	4.07	0.81	
BP Tau	K 7	1.0	2.64	-0.58	
CI Tau	K 7	2.0	2.55	-0.17	
CoKu Tau/3	M 1	5.0	2.66	-1.19	
CoKu Tau/4	M 1.5	3.0	5.37	2.12	
CW Tau	K 3	2.8	1.15	-0.65	
CX Tau	M 0	1.3	2.30	-0.15	
CY Tau	K 7	1.7	0.77	-0.99	
CZ Tau	M 1.5	2.4	2.40	-1.04	
DD Tau	M 3.5	1.0	1.10	-0.74	
DE Tau	M 0	1.2	1.81	-0.13	
DF Tau	M 0	1.6	0.83	-1.09	
DG Tau		1.6	0.13	0.15	
DH Tau	M 0	1.7	3.57	0.26	
DK Tau	M 0	1.3	3.79	-0.80	
DL Tau	K 7	1.5	0.51	-0.77	
DM Tau	M 1	0.7	5.80	1.29	
DN Tau	M 0	0.6	1.06	-0.42	
DO Tau	M 0	2.0	0.94	-0.13	
DP Tau	M 0.5	0.6	1.70	-0.33	
DQ Tau	M 0	1.6	0.65	-0.41	
DR Tau		1.2	1.23	-0.40	
DS Tau	K 5	1.1	2.35	-0.96	
F 04101+ 3103	A 1	1.9	4.46	-0.08	
F 04147+ 2822	M 4	2.5	2.55	-1.11	
F 04192+ 2647		0.0	1.17	-0.47	
F 04262+ 2654		0.0	0.78	-0.13	
F 04297+ 2246A		0.0	3.93	-0.41	
F 04570+ 2520		0.0	0.94	-1.60	
FM Tau	M 0	1.4	3.13	-0.16	
FN Tau	M 5	1.4	1.84	-0.05	
FO Tau	M 2	3.0	1.40	-0.32	
FP Tau	M 4	0.0	0.94	-0.10	
FQ Tau	M 2	1.9	1.23	-0.46	
FS Tau	M 1	1.4	1.28	0.08	
FT Tau	C	0.0	1.86	-0.46	
FV Tau	K 5	5.3	1.47	-0.66	
FX Tau	M 1	2.0	4.04	-0.39	
FZ Tau	M 0	3.7	1.26	-0.87	
GG Tau	M 0	1.0	2.82	-0.31	
GH Tau	M 2	1.0	1.42	-0.33	
GI Tau	K 6	2.3	2.65	-0.63	
GK Tau	M 0	1.1	4.60	-0.37	
GM Aur	K 3	1.2	5.07	1.75	
GN Tau	M 2	3.5	2.93	-1.01	
GO Tau	M 0	2.0	1.99	0.03	
Haro 6-13	M 0	11.9	3.87	0.38	
Haro 6-37	K 7	3.8	1.38	-0.85	
HK Tau	M 0.5	2.7	1.80	0.74	
HN Tau	K 5	1.5	2.44	-0.45	
HO Tau	M 0.5	1.3	2.46	-0.63	
HP Tau	K 3	2.8	2.43	-0.01	
HQ Tau		0.0	3.05	-0.64	
IP Tau	M 0	0.5	4.18	-0.09	
IQ Tau	M 0.5	1.4	1.75	-1.00	
IS Tau	M 0	3.2	2.30	-1.21	
II Tau	K 2	3.8	1.12	-0.87	
LkCa 15	K 5	1.2	6.70	0.62	
MHO 3	K 7	8.3	5.93	0.27	
RW Aur A	K 3	0.5	1.25	-0.54	
RY Tau	G 1	2.2	6.51	-0.09	
SU Aur	G 1	0.9	4.75	0.74	
T Tau	K 0	1.8	-0.27	0.55	
UX Tau A	K 5	0.7	0.78	1.83	
UY Aur	K 7	2.1	2.05	-0.04	
UZ Tau	M 1	1.0	2.25	-0.73	
V 410 A non 13	M 6	5.8	1.70	-0.58	

TABLE 2 | Continued

Name (1)	Spectral Type ^a (2)	A_V ^a (3)	EW (10 m) (4)	n_{13-31} (5)	Median (6)
V 710 Tau	M 1	1.9	1.43	-0.70	
V 773 Tau	K 3	2.0	0.82	-0.85	
V 807 Tau	K 7	0.6	0.67	-0.18	
V 836 Tau	K 7	1.1	3.34	-0.45	
V 892 Tau	B 9	8.0	3.06	-0.13	
V 955 Tau	K 5	3.7	1.54	-0.94	
VY Tau	M 0	1.4	2.34	-0.13	
XZ Tau	M 2	2.9	0.66	-0.32	
ZZ Tau	M 3	1.4	1.01	-0.89	
ZZ Tau IRS	M 4.5	1.5	1.58	0.17	

Note. | See the footnote of Table 1 for an explanation of the table content. Uncertainties in A_V , assumed to be 0.3 mag (Kenyon & Hartmann 1995), account for 15% and 1% of the error bars of EW (10 m) and n_{13-31} , respectively.

^a Spectral type and extinction information were taken from Kenyon et al. (1990); Hartigan et al. (1994); Strom & Strom (1994); Kenyon & Hartmann (1995); Torres et al. (1995); Kenyon et al. (1998); Briceño et al. (1998); Luhman (2000); White & Ghez (2001); Hartigan & Kenyon (2003); White & Basri (2003); White & Hillenbrand (2004); Calvet et al. (2004); Furlan et al. (2006).

TABLE 3
Properties of the targets in the Chamaeleon I region

Name (1)	Spectral Type ^a (2)	A_V ^a (3)	EW (10 m) (4)	n_{13-31} (5)	Median (6)
2M J10580597-7711501	M 5.25	1.6	3.22	0.23	
2M J11062942-7724586	M 6	20.0	1.53	-0.27	
2M J11065939-7530559	M 5.25	0.6	1.70	0.37	
2M J11070369-7724307	M 7.5	16.5	2.60	0.19	
2M J11241186-7630425	M 5	2.7	4.52	0.68	
B 43	M 3.25	8.0	6.98	0.42	
C 1-6	M 1.25	11.6	2.34	-0.55	
C 7-1	M 5	5.0	1.08	-0.54	
Cha Ha1	M 7.75	0.0	1.87	0.00	
Cha Ha2	M 5.25	3.8	1.08	-1.00	
CHSM 7869	M 6	1.6	1.74	-0.57	
CHSM 10862	M 5.75	1.6	0.17	-0.06	
CHXR 20	K 6	3.5	4.28	-0.99	
CHXR 22E	M 3.5	1.4	0.22	0.63	
CHXR 30A	M 0	10.6	2.66	-0.60	
CHXR 30B	M 1.25	11.2	2.99	-0.40	
CHXR 47	K 3	5.1	2.23	-0.66	
CR Cha	K 2	1.5	4.66	-0.14	
CS Cha	K 6	0.3	3.02	2.89	
CT Cha	K 5	1.6	2.14	-0.31	
CU Cha	B 9.5	1.5	-0.49	1.04	
CV Cha	G 9	1.5	5.78	-0.27	
DI Cha	G 2	2.7	1.91	-0.67	
Hn 5	M 4.5	1.1	2.07	-1.45	
Hn 10E	M 3.25	3.6	3.23	0.35	
Hn 11	M 0	7.6	2.56	-0.73	
Hn 13	M 5.75	0.8	1.29	-0.44	
Hn 21W	M 4	2.6	1.45	-0.77	
ISO 52	M 4	1.3	2.20	0.11	
ISO 79	M 5.25	7.9	1.58	-0.14	
ISO 91	M 3	14.5	7.53	-0.40	
ISO 138	M 7	0.0	1.81	-0.27	
ISO 143	M 5	3.0	1.47	-1.01	
ISO 220	M 5.75	6.1	1.44	-0.82	
ISO 225	M 1.75	4.4	1.11	0.15	
ISO 235	M 5.5	7.5	1.48	-1.26	
ISO 237	K 5.5	6.8	3.43	0.51	
ISO 252	M 6	3.4	1.35	-0.85	
ISO 256	M 4.5	9.1	3.27	-0.63	
ISO 282	M 4.75	3.6	1.86	-0.53	
SX Cha	M 0	2.8	2.52	-0.48	
SZ Cha	K 0	1.5	3.38	1.68	
T 5	M 3.25	1.2	1.36	-0.32	
T 21	G 5	3.3	-0.04	-1.05	
T 25	M 2.5	1.6	3.30	2.79	
T 28	M 0	4.8	2.05	-0.60	
T 29	K 6	7.3	2.03	-0.34	
T 33A	G 7	3.0	5.38	-0.54	
T 35	M 0	3.5	0.51	1.49	
T 42	K 5	8.2	1.46	-0.02	

TABLE 3 | Continued

Name (1)	Spectral Type ^a (2)	A_V ^a (3)	EW (10 m) (4)	$n_{13\ 31}$ (5)	Median (6)
T 43	M 2	5.2	1.90	-0.41	
T 45a	M 1	1.9	1.66	0.10	
T 47	M 2	4.2	2.14	-0.28	
T 50	M 5	0.4	2.04	-0.32	
T 51	K 3.5	0.8	4.18	-1.53	
T 54	G 8	1.8	0.62	1.10	
T 56	M 0.5	0.6	7.57	0.90	
TW Cha	M 0	1.2	5.57	-0.18	
UY Cha	M 4.25	0.0	3.10	-0.93	
UZ Cha	M 0.5	2.2	2.13	-0.22	
VV Cha	M 3	0.5	2.43	-0.79	
VW Cha	M 0	2.6	2.52	-0.21	
VY Cha	M 0.5	3.2	2.58	-0.22	
VZ Cha	K 6	2.0	1.35	-0.91	
WW Cha	K 5	4.8	4.16	0.42	
WX Cha	M 1.25	2.0	2.56	-1.03	
WY Cha	M 0	3.0	1.61	-1.18	
WZ Cha	M 3.75	0.5	1.97	-0.75	
XX Cha	M 2	1.2	1.77	-0.39	

Note. | See the footnote of Table 1 for an explanation of the table content. Uncertainties in A_V , assumed to be 0.46 mag (Luhman 2007), account for 10% and 2% of the error bars of EW (10 m) and $n_{13\ 31}$, respectively.

^a Spectral type and, where available, extinction information were taken from Luhman (2004a) and Gomez & Marton (2003). For objects without published or with uncertain extinction values, the optical extinction A_V was derived using the observed optical/near-infrared colors and intrinsic colors based on the spectral type or a typical CTS excess (see text for details).

TABLE 4
Properties of the targets in the Ophiuchus off-core region

Name (1)	Spectral Type ^a (2)	A_V ^b (3)	EW (10 m) (4)	$n_{13\ 31}$ (5)
16126-2235	M 3	0.6	10.98	1.15
16156-2358	F 0	2.2	-0.02	1.36
16193-2314	G 5	3.5	3.47	-0.14
16201-2410	G 0	8.0	6.40	1.32
16225-2607	K 7	1.5	6.89	0.52
16289-2457	G 5	9.5	5.16	0.21
16293-2424	G 0	17.1	2.49	-0.03
Dor 16	K 6	3.8	2.30	-0.03
Dor 28	K 5	2.7	1.85	2.19
IRS 60	K 2	9.0	3.24	-0.49
L 1689SN 02	M 3	15.0	0.45	-0.83
ROX 42C	K 6	1.9	2.08	-0.37
ROX 43A 1	G 0	3.5	5.86	-0.52
ROX 44	K 0	3.8	8.05	0.63
ROX 47A	M 3	1.9	1.20	-0.66

Note. | See the footnote of Table 1 for an explanation of the table content. Uncertainties in A_V , which are typically 0.3 mag (McClure et al., in preparation), account for 10% and 1% of the error bars of EW (10 m) and $n_{13\ 31}$, respectively.

^a Spectral types were taken from Hebig & Bell (1988); Chen et al. (1995); Preibisch et al. (1998); Vieira et al. (2003); Torres et al. (2006); McClure et al. (in preparation).

^b A_V values are from McClure et al. (in preparation).